Characterisation Techniques

Measurements and Interpretation of Electromagnetic Properties

G 2.3 Characterisation of the Transport Critical Current Density for Conductor Applications

Authors: Mark J Raine, Simon A Keys and Damian P Hampshire

G2.3.1 Introduction

There is a large and ongoing international effort to standardise the test and evaluation methods for industrial superconductors (Osamura, 2015). VAMAS (The Versailles Project on Advanced Materials and Standards) and IEC/TC90 (International Electrotechnical Commission/Technical Committee 90) have worked on producing internationally agreed standards for superconductivity that are required to underpin a mature technology and world-wide industry (Gould and Wada, 1995; Tachikawa, 1995). The test methods for measuring the critical current (I_c) of industrial Cu/NbTi, Nb_3Sn, $Bi_2Sr_2Ca_1Cu_2O_y$ (Bi-2212), $Bi_2Sr_2Ca_2Cu_3O_x$ (Bi-2223) and $Y_1Ba_2Cu_3O_{7-\delta}$ (Y-123) composite superconductors have been published as international standards (IEC, 2006c, a, b, 2015). In addition, there has been substantial effort directed at standardising terminology and creating standard test methods for low temperature industrial conductors specifically in the areas of critical current, residual resistivity ratio, copper ratio, mechanical properties and surface resistance (Osamura, Sato et al., 1997; Osamura, 1998), not least because of the industrial needs that have followed from the construction of ITER; the fusion energy tokamak in Cadarache, France (Aymar, Barabaschi et al., 2002; Mitchell, Bessette et al., 2008; Sborchia, Fu et al., 2008; accessed 2016). As part of the development of ITER, seven important characteristics of strand (or wire) conductors were specified

as necessary for the strands to be included in the machine; these are listed in Figure 1 (Sborchia, Fu et al., 2008). As part of the European verification process of the superconducting strands, these seven characteristics were measured by the manufacturers and an independent laboratory in Durham. This article focuses on just one of these measurements – transport critical current (I_c), where techniques are now sufficiently mature that thousands of ductile and brittle samples have been measured by independent laboratories with excellent agreement to within a few percent. The article is written for early career scientists who are new to making critical current measurements.

Practical conductors are used widely today in many large and small scale applications from current leads in satellites (Schlachter, Goldacker et al., 2006) and in CERN (CERN, 2013) to magnets for MRI body scanners and fusion energy tokamaks (Sborchia, Fu et al., 2008; Duyn, 2012; Lvovsky, Stautner et al., 2013). For high field applications, the economic advantage that superconductors offer over copper conductors is the almost complete elimination of power losses in return for an additional cost in cryogenic cooling systems and intelligent systems control. For example, a 20 T, 80 mm bore copper magnet requires several MW of power with a huge cooling system to stop the magnet melting, whereas the equivalent superconducting magnet needs nothing more than a power supply approximating a sophisticated car battery to run.

The most important design parameter in such superconducting systems is the current carrying capacity of the conductor. For many applications, in order to optimise the use of the conductor, one must know this property as a function of magnetic field, temperature and strain. Most of this article describes techniques used to test conductors as a function of magnetic field at cryogenic temperatures. It considers so-called strand conductors which include wires and tapes that typically carry currents of up to 1000 A. Specialist techniques for characterising conductors are also highlighted.

This article has seven main sections. The next one deals with the basic principles behind making a critical current measurement and provides a discussion of the different conventions used to define

the current carrying capacity of a conductor. The subsequent two sections consider the parameterisation and measurement of critical current and then voltage-current characteristics. General considerations for mounting and wiring a sample, eliminating current-transfer problems, and using relevant measuring equipment are addressed. The methods for analysing the data obtained and the information that can be extracted are then outlined. Then we consider a series of case studies and describe good-practice techniques for measuring some of the most important technological materials – NbTi (Lee and Larbalestier, 1987), Nb_3Sn (Taylor and Hampshire, 2005b), Ag-sheathed $Bi_2Sr_2Ca_2Cu_3O_x$ (BiSCCO-2212), Ag-sheathed $Bi_2Sr_2Ca_1Cu_2O_x$ (BiSCCO-2223) (Larbalestier, Jiang et al., 2014; Sato, 2017), as well as RE-$Ba_2Cu_3O_{7-\delta}$ (RE: Rare–Earth, RE-123)(SuperPower-Furukawa, 2013). It refers the reader to specialist techniques that vary considerably from I_c measurements at 4.2 K at the pV m^{-1} electric field level to J_c measurements at the μV m^{-1} level as a function of magnetic field, temperature and strain. The article concludes with a short reflection.

G2.3.2 General Principles for measuring I_c when testing conductors

G2.3.2 Four-terminal critical measurements on strand superconductors

There are many different designs for conductors, from multifilamentary NbTi, Nb_3Sn and BiSCCO strands/wires and tapes to thin film tapes of rare-earth-BCO. Schematic diagrams for some of the most common are shown in Figure 2. In addition to the superconducting filaments one can see the other important components that are part of a technological conductor, including those parts required to fabricate the superconducting material itself (e.g. bronze) or those parts that stabilise the conductor when carrying current (e.g. copper, silver). Some of the most important parameters for describing superconducting strands are listed in Table 1. We can usefully draw a clear distinction between the metallic/intermetallic superconductors and the oxide superconductors that helps to clarify the different approaches to fabricating them and the final forms that result (as shown in Figure 2). The resistivity of the grain boundaries in the metallic/intermetallic superconductors is typically

similar to that of the grains, independent of the angle between neighbouring grains (Byrne, 2017). However, for the oxide materials, low resistivity grain boundaries i.e. strongly coupled grains, are only achieved when the angle between the grains is very small, typically less than five degrees – although low resistivity may also be possible at some higher coincident-site-lattice magic angles (Dimos, Chaudhari et al., 1988). Strongly coupled grains are a necessary but not sufficient requirement for high critical current densities (Wang, Raine et al., 2017). Hence the metallic/intermetallic superconductors can be fabricated to include both high and low angle grain boundaries, whereas in contrast the BiSCCO materials include a very large degree of texturing (forced grain alignment) (Larbalestier, Jiang et al., 2014) and RE-123 production uses thin film fabrication techniques to attain almost exclusively low angle grain boundaries to achieve high critical current densities (Iijima, Tanabe et al., 1992; Goyal, Paranthaman et al., 2004; Durrell, 2009). Proper consideration of the construction of the strand is important when characterising its current carrying capacity (c.f. Section G2.3.3). There are many excellent reviews and texts that discuss conductor design (Wilson, 1986). Nevertheless, the basic principles behind a critical current measurement are the same for all superconductors - those of a text-book four-terminal resistance measurement. The current is applied to the sample by means of current contacts at both ends and the voltage is measured across a pair of taps positioned across a length of the sample between the current contacts. The current is slowly increased from zero and the voltage across the taps is monitored. Eventually a *V-I* (or equivalently an *E-J*) characteristic is measured. This process can be repeated as a function of applied magnetic field as illustrated in Figure 3, which includes a block diagram of a typical experimental arrangement and data. For the data shown, an *E*-field criterion of either 10 $\mu V\,m^{-1}$ or 100 $\mu V\,m^{-1}$ are common choices (c.f. Section G2.3.3) used to obtain the critical current density.

G2.3.2.1 Sample geometry and wiring

There are three sample geometries that are most commonly used for measuring critical current. Some of the different forms are shown in Figure 4. The choice of geometry mainly depends on the architecture or form of the superconductor, which includes considering the magnitude of the critical current to be measured and whether the superconductor has significant anisotropy. Here we call the geometries; “straight”, “hairpin” (or “U-bend”) and “coil” geometries. The straight geometry is most often used for conductors that are still in early development, where homogeneous lengths - typically sintered blocks of conductor - are the only form available. The hair-pin geometry is used for samples that carry high currents, where current-transfer from the current leads into the conductor are a problem, usually because it is difficult to make low resistance/high current connections (c.f. Current-transfer section in G2.3.2). The coil geometry is commonly used to test long lengths of conductors; usually for technologically mature materials that are available commercially.

G2.3.2.2 Straight geometry

The short straight geometry is the simplest configuration. The short sample fits into the bore of a solenoid magnet, as shown in Figure 4a and Figure 4b. For broadly isotropic materials, this is the standard orientation of field and current flow because the direction of current flow is perpendicular to the applied magnetic field. This orientation gives the lowest critical current, and therefore provides the most useful (limiting) case for high field applications (Goodrich and Fickett, 1982; G. Grasso, 1997). The short sample geometry provides the least sensitive *E*-field criterion for the determination of J_c because of the short measuring length between the voltage taps. The orientation of the sample to the current leads also means that there is a relatively small contact area for the current to transfer into the sample compared with the other configurations. This, in turn, increases the contact resistance and heating. The reduced space around the sample limits the distance over which the current can distribute into the superconducting filaments. If the current has not

transferred into the superconducting filaments, the voltage recorded across the taps is associated with the current that has remained in the normal matrix. Hence, voltage taps need to be sufficiently separated from each other to allow sensitive *E*-field measurements to be made, but also sufficiently separated from the current leads to avoid the problem of current-transfer voltage. Current-transfer into the superconducting filaments is an important problem for measurements on small samples as discussed below. No bending of the sample is required during mounting. The sample is easily supported against the Lorentz forces present when performing critical current measurements in applied magnetic fields, which is particularly important for brittle superconductors. The width of the bore (or cryostat tail) obviously provides a limiting size. A much greater length of sample can be used in the long straight geometry, as shown in Figure 4b. The voltage taps are in the homogenous region of the magnet and are well separated from the region where the current-transfers from the current leads into the superconductor. Also, a greater length of the sample is in contact with the current leads. This larger contact area reduces contact resistance and hence heating in this area. The longer length provides a longer measuring region for the voltage taps, leading to increased *E*-field sensitivity. The homogeneity of the magnet determines the maximum length over which the voltage taps can be placed. For anisotropic materials, the geometry in Figure 4c is important because as the sample is rotated, the direction of current flow remains orthogonal to the applied field and the anisotropy of J_c results from the superconducting materials anisotropy. Note that measurements using split-pair or Helmholtz type magnets are relatively rare, because such magnet systems are more expensive than vertical magnets - the forces in them are higher and hence more difficult to manage and the stored energy is generally larger, so the amount of superconducting material required for a given maximum field and bore size is larger. Figure 4b shows how the short sample geometry can be used with a split pair magnet to measure the dependence of critical current on the orientation of current flow with respect to the direction of the applied field. This geometry is used to measure the effect of the mean Lorentz force changing from a maximum value to zero. This anisotropy is usually low, typically less

than a factor 2, associated with the tortuous local current density flow, the large range in the directions of flux flow and the vector nature of the local Lorentz force.

G2.3.2.3 Hairpin geometry

The hairpin geometry shown in Figure 4d reduces the contact resistance between the leads and the conductor and hence reduces current-transfer effects - similar to the long straight sample geometry but without requiring a split-pair magnet. As the current leads are not near the voltage measurements region, a longer measuring distance between the voltage taps can be used and hence a better *E*-field sensitivity is achieved than in the short straight geometry. The hairpin geometry is suitable either for ductile superconductors such as NbTi or for conductors that can be reacted into the required shape (e.g. Nb_3Sn) - but clearly remains problematic in the latter case if the reaction process is commercially sensitive (e.g. BiSCCO). This geometry is clearly not suitable for conductors that do not meet one of these two criteria because the strain produced in the sample on forming this configuration usually damages the sample. Another aspect of this geometry is the curved nature of the sample. If the orientation of the conductor between the voltage taps varies with respect to the direction of applied magnetic field (e.g. the conductor is of semi-circular shape) then the critical current measured will represent an angular average over the applied field. A flat-bottomed hairpin is therefore preferable to a round-bottomed hairpin. However, particular care must be taken to avoid damaging the sample when fabricating flat-bottomed samples.

G2.3.2.4 Coil Geometry

The coil geometry (Figure 4e) is most commonly used for testing long lengths of conductor. It is suitable for ductile materials and conductors that can be reacted in the coil shape – most obviously, the ductile alloy NbTi which is the workhorse material for applications below 10 T and the brittle intermetallic Nb_3Sn which is currently the LTS material of choice for applications above 10 T. The

length of conductor used is the largest of all geometries. The voltage taps can be placed the greatest distance apart (typically 0.5 m), leading to the best *E*-field sensitivity. The contact resistance and the current-transfer effect can be largely removed for this arrangement. Although the sample is oriented at an angle to the applied magnetic field, all parts of it experience the same offset angle, which generally has little effect. For example, in Nb_3Sn, a 7° pitch represents a change in I_c of only 2% (Goodrich and Fickett, 1982). The coil geometry also provides the opportunity to investigate the homogeneity of the conductor by placing multiple sets of voltage taps along the sample.

G2.3.2.5 Voltage wiring

There are many sources of voltage noise that can affect J_c measurements. The largest are usually eliminated by twisting the voltage tap wires together and tying them down in order to prevent them from producing inductive voltage noise by moving in the magnetic field caused by cryogenic gas flow. The area between the voltage wires and the sample should also be minimised to reduce the inductive loop area further. This procedure minimises inductive voltages which are produced either as the current through the conductor is increased or from the ripple in the applied magnetic field. For straight and hairpin samples, the voltage wires simply run along the surface of the conductor, as shown in Figure 4. For the coil geometry, where the distance between voltage taps can be several turns, the wire from the first voltage tap should run alongside the sample until the second voltage tap, as shown in Figure 4f. From there, the wires should be twisted together. Other sources of voltage noise include thermoelectric, offset, ground loop, common mode and current-transfer voltages (Goodrich and Bray, 1989). If these voltages stay constant during the measurement then they can easily be subtracted from the data. This is achieved by comparing the voltage at zero current before and after the trace is measured. For the most sensitive voltage measurements, the twisted pair of voltage wires should be continuous from the sample to the voltmeter. In this case the thermoelectric voltages are minimised since there are no joints along the length of the voltage wires. We recommend

measuring the voltage noise in measurements and comparing it with the fundamental Johnson noise associated with quantisation of charge. The root-mean-square (rms) voltage from Johnson noise is given by

$$V_{\mathrm{rms}} = \sqrt{4k_{\mathrm{B}}TR(\Delta f)}, \tag{1}$$

where k_{B} is the Boltzmann constant, T is the temperature of the voltage leads, R is the resistance of the voltage leads and Δf is the inverse of the time constant of the voltmeter/amplifier. In high field critical current measurements, we find the experimental noise is typically five times the fundamental noise floor.

G2.3.2.6 Current leads

The design of the current leads varies widely, depending on the application (Sunwong, Higgins et al., 2014). The temperature gradient along sophisticated current leads, for example, can be controlled by more than one cryogenic liquid and/or the operation of a cryocooler. In general, current leads must transport sufficiently large current without thermal runaway or burnout, have low electrical resistance so they do not generate much additional heat in the system and have low thermal conductivity to minimise static boil-off. Unfortunately, a room-temperature superconductor, which may have ideal properties for current leads, has not yet been discovered. Nevertheless, the high temperature oxide superconductors can be used to reduce power consumption in current leads significantly and hence operating costs in large scale cryogenic systems. Here some general design principles are considered for current leads. We will provide order of magnitude values for the size of current leads to aid those new to these measurements. For some detailed analysis, the reader is referred to the excellent work in the literature (Wilson, 1986; Herrmann, 1998; Sunwong, Higgins et al., 2014).

In simple terms, the design of the current leads can be separated into four sections: (I) The connection from the power supply to the probe. Generally, there is very little or no gas flow, so one

must ensure the room temperature wiring is rated to carry the maximum current to be used, usually the maximum current the power supply can provide. However, significant reduction in the cross-section of these leads can be achieved if one includes realistic duty cycles for the measurements. For example, we have leads rated significantly below 2000 A d.c. attached to our 2000 A power supplies because most of the experimental time is spent ramping the magnetic field or stabilising the temperature, which provides sufficiently long periods where current is not being carried by the leads, allowing them to cool before the next duty cycle. Typically, I_c measurements only run for $\sim 20\%$ of the time and typical I_c values are around 1000 A and even when measuring the highest I_c values the current flowing is only close to 2000 A for a relatively small fraction of the measurement time. This means we are able to run our current leads hot for short periods. (II) The top section of the current leads inside the probe – operating at an approximate temperature range from room temperature or higher, down to 200 K. This section is inside the probe, from the head of the probe (where the room temperature power supply leads are connected) down to a level close to the neck fitting at the top of the Dewar. Our experience is that this region is the most likely to burn out. Efficient use of the cryogen exhaust keeps the leads as cool as possible. The leads are usually best made of copper with a cross-sectional area similar to that of the brass leads located in the middle section of the probe. (III) In the middle section, there is a temperature difference from about 200 K down to the temperature of the cryogen. One must ensure that all the available enthalpy from the cold flowing cryogenic vapour is used to cool the leads in this region. In optimal design configurations, brass is often the preferred material. Tubes are used with sufficient bulk to provide a large surface area for efficient vapour cooling, reducing the likely risk of them burning out in comparison to, say, copper, if temporarily operated outside optimal conditions (Herrmann, 1998). An optimised constant diameter brass lead operating from room temperature to liquid helium can efficiently carry a current given by the condition

$$A_{\mathrm{Brass}} = I_{\mathrm{Max}} L/(1.5 \times 10^6), \quad (2)$$

where A_{Brass} is the cross-sectional area of the brass, I_{Max} is the maximum current carried by the lead and L is the length of the lead (Sunwong, Higgins et al., 2014). Hence, for a 1 m lead, the current density in the brass should be 150 A cm^{-2} when the current flowing is at I_{Max}. Under these conditions the leads are sufficiently large that at operating current resistive heating is optimally kept below excessive levels but are also sufficiently small to minimise static helium boil-off. The heat load (Q) into the helium cryogen is typically 1.08 W kA^{-1} or 1.4 l of liquid helium per hour per kA. For brass leads, vapour cooled with a nitrogen cryogen, $IL/A \sim 8 \times 10^5$ A m^{-1} and $Q = 25$ W kA^{-1} [9]. This middle section can also have high temperature superconducting tapes or multifilamentary conductors soldered in parallel to minimise heat generation. (IV) The leads in the bottom section of the probe, which are submerged in the cryogen, should be relatively bulky to minimise resistive losses and incorporate superconducting (usually oxide and metallic/intermetallic) wires in parallel. The leads should also be large enough to prevent film boiling of the liquid cryogen (Wilson, 1986). During film boiling, the lead is enveloped by a layer of insulating gas which results in a rapid temperature rise of the current lead, possibly leading to an undesirable increase in sample temperature (Sakurai, Shiotsu et al., 1996).

The reader should be careful with the use of flat oxide tapes (i.e. non- multifilamentary tapes) in horizontal split-pair magnets. The stray field in such magnets is large and can magnetise the tapes in the current leads. It takes a considerable torque to rotate these magnetised tapes in-field and therefore, probes with such tapes incorporated within their current leads can only be rotated in low fields.

G2.3.2.7 Sample holder – bonding, thermal contraction and resistivity

Experimental testing of conductors can involve making nanovolt measurements in high magnetic fields with hundreds or thousands of amps flowing through the conductor. The brittle nature of some

conductors, and the high Lorentz forces present, mean that the conductor must be fastened securely to prevent the sample from moving and subsequently becoming damaged. Even for ductile conductors, sample movement may also lead to additional voltage noise, variations in the measured critical current, or even thermal runaway below I_c.

For straight and hairpin geometries, the sample is simply mounted onto the planar surface of the sample holder after reaction or fabrication. For the more complicated coil geometry, ductile samples are wound directly onto the cylindrical sample holder for testing. For brittle materials, samples are either directly reacted on the sample holder or (although less preferred) reacted on a mandrel in the furnace and then carefully transferred, after reaction, onto the sample holder. The direction of the Lorentz force is orientated so that it presses the sample against the sample holder and facilitates using less bonding agent to hold the sample in position. Bonding agents include G.E. Varnish, epoxy (such as Stycast), vacuum grease and solder. A high strength bonding material (e.g. epoxy or solder) is required if large Lorentz forces are present; although completely covering a sample with excess bonding agent must be avoided since this will inhibit the transfer of heat from the sample to the cryogen and can reduce the maximum measurable critical current.

It is also often important to try to match the coefficient of thermal contraction for the sample holder to that of the sample. This ensures that there is no additional stress applied to the sample, which may affect I_c when the sample is cooled from room temperature (or the soldering temperature if solder is the bonding agent) to the cryogenic testing temperature. The coefficient of thermal contraction, for some important cryogenic materials, is shown in Figure 5. Figure 5a shows thermal contraction data for various superconducting compounds, composites and matrix materials (Clark, Fujii et al., 1981; White, 1987; Meingast, Kraut et al., 1991; Okaji, Nara et al., 1994; White, 1998; Yamada, Nara et al., 1998). It should be noted that the thermal contraction of the wire will depend ultimately on the construction of the whole composite (Ochiai, Osamura et al., 1993; Osamura, Machiya et al., 2014; Osamura, Machiya et al., 2016). In the VAMAS work, contractions of 0.26% to

0.28% were reported from room temperature to 77 K (Goodrich and Srivastava, 1995b; Kirchmayr, Siddall et al., 1995). Figure 5b shows the thermal contraction for various common mandrel or bonding materials (Clark, 1983; Pobell, 1996; White, 1998; Cheggour and Hampshire, 2000). This parameter for G10-CR and G11-CR is similar in the fill and warp directions. The difference between the thermal contraction of the sample holder and the sample is transmitted between the two by the bonding agent. If a large amount of bonding material is used, both the sample holder and bonding material contribute to the net stress on the sample. The stronger the bonding material, the greater the strain produced by any differential thermal contraction between the sample holder and conductor. The type of bonding agent used must therefore be considered carefully for each particular experiment (see case studies below).

The most often used materials for the sample holder are the insulating composite G10, the highly resistive Ti-alloy, Ti-6Al-4V (Ti-64) and Cu-Be, which has a high elastic limit of ~ 1% at 4.2 K (c.f. Figure 6 and Figure 7). Although Ti-64 alloy is widely used, at 4.2 K and below 3 T it becomes superconducting and Ti-6Al-2Sn-4Zr-2Mo-0.2Si (Ti-6242) can be a better choice(Ridgeon, Raine et al., 2017). Cu-Be is also often used as a sample holder because one can easily solder the sample to it, minimising sample movement, and because of its high elastic limit (Cheggour and Hampshire, 2000). However, at 10 K the resistivities of the Ti-alloys are about $1.5 \times 10^{-6}\ \Omega\,\mathrm{m}$ whereas Cu-Be is much less resistive at $4.7 \times 10^{-8}\ \Omega\,\mathrm{m}$, so one has to be careful about current shunting through the sample holder as the superconductor becomes resistive at I_c (Ridgeon, Raine et al., 2017). As discussed below, although the shunting might only produce a small error for correction for I_c, it can significantly affect the measured *n*-value.

G2.3.2.8 Current-transfer in composites

Consider two types of current-transfer: The first of these is the initial transfer of current from the current leads into the conductor. Best results are obtained if both the leads and the sample can be

separately tinned (coated in solder) and then sweated (heated while applying pressure) together so that there is good electrical contact with little excess solder. This ensures that there is a low resistance path from the copper parts of the leads to the sample/filaments of the wire, and that any heat generated can easily be conducted into the helium bath without heating the wire excessively (avoiding quenches). Measurements of J_c are most reliable with the voltage taps as far away as possible from the current-transfer regions near the current leads. This ensures that the properties of the conductor alone are measured, rather than the properties of the current lead joint resistances. The voltages produced in the current-transfer region, across the matrix of the superconducting wire or tape, increase linearly with current (unless, of course, there is heating in the sample). It has been shown (Ekin, 1978) that the distance required to allow for current-transfer to a monocore conductor is given by

$$L = d\sqrt{\frac{0.1\rho_m}{n\,\rho^*}}, \tag{3}$$

where d is the diameter of the filament region of the wire (i.e. the area of the wire containing the superconducting filaments), n is the order of transition which describes the shape of the *V-I* curve for the superconductor (c.f. section G2.3.3), ρ_m is the resistivity of the matrix, and ρ^* is the resistivity criterion used to define the critical current density. This equation yields typical current-transfer distances of approximately $30d$ for Nb_3Sn and $3d$ for NbTi (Goodrich and Fickett, 1982). The increased current-transfer length for Nb_3Sn compared with NbTi is due to the lower values of n (i.e. 20 for Nb_3Sn compared to 40 for NbTi), and the large resistivity of the matrix (bronze for Nb_3Sn compared to pure copper for NbTi). Unfortunately, as Pauli is famously quoted as saying, 'God made the bulk; surfaces were invented by the devil' and Eq. (3) must be considered a minimum distance. In BiSCCO 2212 and 2223, the transfer lengths are typically a millimetre at 4.2 K, and tenths of millimetres at 77 K (Polak, Zhang et al., 1997). They have an unexpected temperature dependence which is attributed to a large boundary resistance at the interface between the superconductor and

the silver sheath. In RE-123 tapes, detailed measurements have shown that the interfacial resistivity between the superconductor and the silver layers is 25 $n\Omega\,cm^2$ (Tsui, Surrey et al., 2016). The current-transfer lengths directly affect the choice of sample geometry. Samples are typically no longer than 35 mm in the short straight geometry. This means that measurements on conductors with high resistivity matrix (e.g. bronze route Nb_3Sn) are best not made using the short sample geometry. However, because the current-transfer is not an intrinsic property of the wire, the resistive voltage can be subtracted from the *V-I* trace (Ekin, 1989). Note that when testing conductors with twisted filaments (which is required in commercial conductors to minimise a.c. losses), the current contact length should be greater than the twist pitch of the sample to allow the current to enter the filaments evenly (Goodrich, Ekin et al., 1982).

The second current-transfer process is interfilamentary and occurs along the entire length of the conductor. It is generally due to a distribution in I_c. This process depends on the detailed structure and materials in the composite conductor, including the size and distribution of the filaments within the conductor matrix and is an intrinsic property of the conductor. It is particularly important for a.c. applications where currents can redistribute between the filaments. In d.c. applications, a quantitative picture of the dissipative state in inhomogeneous high J_c conductors depends on the *E*-field range under investigation. At low *E*-fields, for example in NMR (or persistent mode) applications, the superconducting filaments may have a resistance that is still much smaller than that of the matrix. In this case, the *V-I* transition is largely unaffected by the matrix and the current-transfer is not important. In high *E*-fields, sausaging of the filaments or inhomogeneities may mean the local I_c in a filament is exceeded, current passes through the matrix, either back into the sausaged filament or into another filament (Polak, Zhang et al., 1997).

G2.3.2.9 Current source and voltmeter

A current source that can smoothly ramp current up and down, and a nanovoltmeter are typically used under computer control for making J_c measurements. The current through the sample is usually recorded by measuring the voltage drop across a standard resistor, and the voltage across the sample by the nanovoltmeter, as shown in Figure 3. The sensitivity and response time of the nanovoltmeter is dependent on the quality of the instrument and the filters used. Voltages at about 100 nV can be measured over an interval of around 50 ms. Standard good practice must be observed when using filters to reduce the voltage noise on a *V-I* characteristic. In general, the greater the filter used, the larger the time delay before the correct voltage reading is reached. If the response time of the filtering mode is too long, the apparent voltage will be less than the actual voltage, and the *V-I* transition will artificially broaden giving a false increased value for I_c (and a decreased *n*-value – c.f. Section G2.3.4). Measurements below the 10 nV range are possible in low noise systems with long measurement times. Noise levels can be improved if outlying points are removed and numerical smoothing implemented (Goodrich and Srivastava, 1990). The current source itself can be a source of voltage noise. For example, it has been found that a battery power supply gave a noise level during the measurement of ~ 2 nV, whereas a silicon controlled rectifier gave ~ 100 nV (Goodrich and Fickett, 1982).

In the most widely used measurement technique, the current is simply ramped at a constant rate until the required voltage is generated across the sample. The measurement should be sufficiently slow that the *V-I* trace does not depend on the rate of increase of current. The rate of increase of current must be small enough that the generated inductive voltages vary by less than the voltage used to determine J_c. Other factors that limit the ramp rate or the current are possible sample movement and induced eddy currents in metallic sample holders and probe components which cause heating. In the stepped method technique, point-wise data are taken with a delay to allow the inductive voltage to decay. A third method is to ramp quickly to $\sim 0.9 I_c$, wait for the inductive voltage

to decay and then sweep the current very slowly through the I_c transition. Pulsed techniques are also used (c.f. section G2.3.4), and at high *E*-fields, typically agree with d.c. methods to better than ~ 0.2% (Goodrich, 1991) but usually with higher noise levels. A calibrated superconducting simulator is available to assess experimental procedure (Goodrich, Wiejaczka et al., 1995).

Most experimental arrangements also incorporate some form of quench protection device. This is particularly important when using unstabilised samples where there is a significant risk of burning out the sample. The protection automatically resets the current to zero when a pre-determined voltage across the sample is reached. Both computer controlled and free-standing independent analogue components have been used to provide quench protection (Goodrich and Fickett, 1982).

G2.3.2.10 Magnetic field

The magnetic field applied to the sample during critical current measurements is often provided by using a superconducting magnet. Dedicated University and National Laboratories often include vertical solenoidal magnets producing fields of up to ~ 23 T and horizontal Helmholtz split-pair magnets up to 15 T. In the VAMAS Nb_3Sn project, it was recommended that: the field for testing conductors should be accurate to 1% and have a precision of 0.5%; the random deviation of magnetic field should be less than 0.5% and its homogeneity should be of uniformity ±1% over the length of the sample between the voltage taps (1995).

Above ~ 1 T, high field superconducting magnets exhibit an almost linear dependence between the field generated and the current through the magnet. At low fields, however, hysteresis can cause problems when trying to determine the low field properties of conductors. There are various approaches that can be taken to eliminate errors due to the remnant field. The field at the sample can be measured independently using a Hall or NMR probe. The remnant field can be reduced to typically less than ± 20 mT by degaussing the magnet. This involves sweeping the field from a high value through zero and back, reducing the amplitude and sweep rate at each reversal. An alternative is to

initiate a controlled quench in the magnet. This can be done by means of a carefully designed quench heater (Clark and Jones, 1986) incorporated within the turns of the magnet which forces the temperature of the superconducting windings above T_c. This completely destroys the remnant field. However, the dangers of damaging the magnet by quenching should be noted.

At international high field laboratories, d.c. fields of up to ~ 45 T are produced by high power resistive magnets (Miller, 2003; Pugnat, Barbier et al., 2014). These conventional magnets in principle have no remnant field, although in practice the structural steel in these systems is magnetised. The water cooling and power required for this design of magnet are large, which causes mechanical vibrations in the magnet system and additional sources of voltage noise. Wholly superconducting HTS and LTS magnets have been produced. HTS magnets operating up to 26.4 T have now been produced (Yoon, Kim et al.; Awaji, Watanabe et al., 2017) as well as many insert systems such as the 35.4 T high field magnet produced by a 4.4 T RE-123 insert inside the bore of a 31 T LTS magnet (Trociewitz, Dalban-Canassy et al., 2011).

G2.3.3 Critical Current Density – parameterisation and measurement

The basic process that leads to an electric field being generated along the superconductor when the critical current density is flowing, is well understood. In a superconductor, the current density is confined to the superconductor and there is a Lorentz force between the flowing current density and the fluxons. As the current density through the wire is increased, the Lorentz force increases until it is sufficiently large to unpin the fluxons. When the fluxons move, they generate an electric field in agreement with Faraday's law (Bardeen and Stephen, 1965). Early experimental and theoretical work found universal scaling laws for the volume pinning force density that are still used to parameterise J_c in technological low temperature superconductors given by

$$F_P = J_c B = A \frac{[B_{c2}^*]^n}{[\kappa_1^*]^m} b^p (1-b)^q, \quad (4)$$

where $b = B/B^*_{c2}(T,\varepsilon)$, $\kappa_1^*(T,\varepsilon)$ is the effective Ginzburg–Landau parameter (Keys and Hampshire, 2003) and $B^*_{C2}(T,\varepsilon)$ is the effective upper critical field. The compilation of different pinning mechanisms that Dew-Hughes produced (Dew-Hughes, 1974) has helped shape the use of Eq. (4). He found that for a wide range of model pinning systems, consistent with general dimensionality arguments that consider the Ginzburg-Landau free-energy functional, that m = 2 or greater and n, p and q have integral or half-integral values. Experimental work provided broad confirmation of both temperature scaling and strain scaling predicted by Eq. (4), although initially with the non-physical result that n was different for data taken at fixed temperature and different strain values ($n \sim 1$ for strain scaling) (Ekin, 1980) compared to data taken at fixed strain for different temperatures ($n \sim 2$ for temperature scaling) (Hampshire, 1974). These differences in the exponent n were resolved with variable strain and variable temperature measurements on a single wire. They provided a unified scaling law consistent with Eq. (4) when the strain and temperature dependence of the Ginzburg-Landau parameter (Hampshire, Jones et al., 1985) were included (Cheggour and Hampshire, 1999).

There is now such a vast amount of J_c data on low temperature superconductors that are consistent with Eq. (4), that the language of "flux pinning" has continued to be used to explain critical current density in systems using the very useful early ideas, from many different authors (Campbell, Evetts et al., 1968; Dew-Hughes, 1974, 2001), of fluxons ripped out of free energy wells or pinning sites. However, they do not provide a very accurate description of the dissipative state. For example, later work, notably by Kramer, included the role of fluxon-fluxon interactions that occur in the flux-line-lattice, ranging from his work on flux shear models in an almost perfect flux-line-lattice (Kramer, 1973, 1975) to collective pinning models with good short and intermediate range order in the flux-line-lattice but no long range order (Larkin and Ovchinnikov, 1984; Feigel'man, Geshkenbein et al., 1989). The important "pinning" in such models then becomes associated with the strength or elastic constants of the flux line lattice (Hampshire and Jones, 1987c), rather than a particular feature of the microstructure. This work highlighted what has been called the 'grand summation problem' which

considers the difficult issue of how to sum the forces in the flux-line-lattice correctly to obtain J_c.(Antesberger and Ullmaier, 1975). It raises questions such as whether one should consider the fluxons to be in a broadly perfect hexagonal lattice or in an amorphous structure (Kleiner, Roth et al., 1964) and what the nature of fluxon movement after depinning is. Computational solutions to the time-dependent-Ginzburg-Landau (TDGL) equations for polycrystalline materials suggest that flux flow at criticality in polycrystalline materials is complex. There are broadly two distinct regions – grain boundaries which flux most easily penetrates and that provide channels along which flux traverses the superconductor at criticality and the interior of the grains where flux broadly does not move at criticality (Carty and Hampshire, 2008).

It is difficult to find a simple accurate functional form to parameterise J_c in high temperature superconductors, not least because of the anisotropy of these materials, the much larger effect of compositional variations on superconducting properties and the complexity of the microstructures that are being used to produce high J_c (Carty and Hampshire, 2013; Sunwong, Higgins et al., 2013). In high field superconductors, where the coherence length can be a few nanometres, we need to understand changes at the atomic scale. These are unsolved and challenging problems even for low temperature superconductors, where historically there has been a consensus that BCS theory describes the fundamental pairing mechanism (Bardeen, Cooper et al., 1957). For high temperature superconductors, where there is no agreement about the origin of the superconductivity, the deficiencies in our understanding are even more severe since we do not know how the pinning sites (e.g. grain boundaries, inclusions and precipitates) affect the local superconducting properties (Uemura et al, 1989; Uemura, Le et al., 1991). Nevertheless, despite the huge gaps in our understanding of J_c, the community is firmly committed to producing, not just descriptive, but also predictive tools that relate the structure and microstructure to the critical current density. This is not least because Ginzburg-Landau theory reminds us that J_c, even in state-of-the-art high-field technological superconductors, is still typically more than two orders of magnitude below the

theoretical limit at $0.5B_{c2}$ as shown in Figure 8. One may expect that this huge headroom will only close as we move away from polycrystalline superconductors towards single-crystal materials with strong pinning, as has been so effective in increasing J_c in RE-123 materials (Wang, Raine et al.) (Hazelton, 2013). Fortunately, the technological development of superconductivity has progressed successfully even with the current (relatively low) values of J_c and has not prevented the development of a multi-billion dollar industry (Conectus, 2001).

G2.3.3.1 Defining the critical current (I_c) and the critical density (J_c)

A generic voltage-current (*V-I*) characteristic is shown in Figure 9 along with the various conventions used to define the critical current. The choice of convention depends on how the data are to be used. For example, in standard high field solenoids the engineering current density at an electric field criterion of about 10 μV m^{-1} will determine the performance of the magnet. For NMR applications, on the other hand, where the magnet is in persistent mode, the current density at an *E*-field about six orders of magnitude lower is required. The critical current is consequently dependent on the chosen criterion (Goodrich and Fickett, 1982).

The most commonly used convention for defining critical current (I_c) is an electric field criterion (E_c) given by $E_c = V/L$, where *V* is the voltage difference between the voltage taps and *L* is the length of wire between the voltage taps. Typically, the electric field used to define I_c is 10 μV m^{-1} or 100 μV m^{-1}. I_c never falls to zero, using such criteria. A resistive (ohmic) sample which has no curvature on the *V-I* trace will still cross the electric field criteria at some finite current, leading to a value of I_c. For typical conductors (~1 mm diameter), this non-superconducting current (for example in the Cu that stabilises the conductor) ranges from 10 – 500 mA when the *E*-field is 10 μV m^{-1}, which is not significant in engineering applications. It can be important for more fundamental studies where one is trying for example to measure the upper critical field, since low current densities obtained using this criterion can be characteristic of non-superconducting component metals. In the case of short

straight geometry where the measurement distance is typically no longer than 1 cm, a voltage sensitivity of less than 100 nV is required to obtain an electric field criteria of 10 μV m^{-1}, so often 100 μV m^{-1} or even a 1000 μV m^{-1} electric field criterion is used.

The resistivity criterion (ρ_c) is given by $\rho_c = VA/IL$, where V is the voltage difference between the voltage taps, L is the length of the wire between the voltage taps, A is the cross-sectional area of the wire and I is the current through the wire, is also used. Values of J_c are often quoted at ρ_c of 10^{-14} Ω m or 10^{-13} Ω m. The critical current using the resistivity criteria is eventually zero in high enough fields as long as the criterion chosen is less than the normal state resistivity of the composite conductor. However, problems can also arise in fundamental studies if the resistivity criterion is used. For example, some superconductors have some parts of their superconducting field-temperature phase space, where flux creep dominates and the critical current is zero, showing a low but non-zero resistance region in high fields. If the (superconducting) flux flow region has a resistivity above that of the resistivity criterion, I_c is zero but the conductor remains in the superconducting state (i.e. there are still paired superelectrons). If the resistivity of the sample is below that of the criterion chosen, the analysis suggests a critical current is present although the sample is resistive.

A power criterion (P_c) defined by $P_c = IV$, is sometimes used in large scale applications. It can be a useful criterion in magnet design to specify the maximum allowed consumption of cryogen and thus a suitable working current.

The offset method (Ekin, 1989) is a method for calculating I_c that attempts to minimise the problems associated with the electrical field or resistivity criterion. I_c is calculated in two stages. A tangent to the *V-I* curve is constructed at an electric field criteria given by J_c. The critical current is then defined as the current at which the tangent is extrapolated to zero voltage. This procedure provides an attempt to subtract the current flowing in the non-superconducting components from

the total current which can be useful for samples where there is a large shunt in parallel with the superconductor. We do not recommend using the offset method unless it cannot be avoided.

The critical current density can be calculated in three ways once the critical current has been measured. For engineering applications, the conductor is treated as a single entity. The *V-I* characteristic for the entire conductor, including the stabilising material and the matrix, is required. The engineering critical current density (J_c^{ε} or J_e) is defined as the critical current divided by the cross-sectional area of the entire conductor. This is the important parameter when designing systems such magnets. The second definition of current density is relevant for comparing and developing conductors of different superconducting materials. It can be seen in

Figure 2 that, in contrast to NbTi and BiSCCO, Nb_3Sn conductor has matrix material such as (tin depleted) bronze, which is neither superconducting nor contributes to stabilising the conductor. However, it is required in the processing of the conductor and cannot be removed. Hence the so called 'non-copper critical current density', $J_{c(Non\text{-}Cu)}$, can be calculated using the area of the superconductor that is not matrix material (i.e. non-Cu or non-Ag). This provides the second definition of J_c and is particularly useful for wire manufacturers. In fundamental studies, the critical current density in the superconducting layer alone is required. Measuring the cross-sectional area in NbTi or BiSCCO is relatively straightforward. However, if there are fine superconducting filaments, as in Nb_3Sn or Nb_3Al conductors, it can require electron microscopy or post measurement etching techniques to determine the cross-sectional area of the superconducting layers alone (Raine, T et al., 2017).

G2.3.4 Voltage-Current Characteristics – parameterisation and measurement

G2.3.4.1 Shape of the transition - flux flow, flux creep and damage

In this section the challenges interpreting the shape of the *V-I* traces are discussed. Poor experimental technique can produce artefacts in the data which can be very misleading, particularly when

measuring brittle superconductors. Figure 10 shows five *V-I* characteristics that will be discussed in this context. These data are schematic representations of actual characteristics with their important features enhanced, and can be explained as follows:

Figure 10(a) There is a resistive (current-transfer) region at low currents due to an insufficient separation between the current leads and the voltage taps. The transition to the normal conducting state is evident at high currents.

Figure 10(b) Flux creep is evident at low currents. At high currents, the transition rises sharply as flux flow sets in.

Figure 10(c) At low currents a negative thermal voltage is developed. This can occur if there is excessive heating at one end of the sample where the current is injected, and can cause a significant temperature gradient between the voltage taps. At intermediate currents, the voltage can become net positive due to resistive voltage associated with current-transfer in and out of a limited number of damaged filaments. At high currents, the conductor is in the flux flow state.

Figure 10(d) There is zero resistance region followed by a flux flow transition.

Figure 10(e) There is zero resistance until a quench occurs in the conductor. This is followed by heating and thermal runaway leading to an artificially high *n*-value (c.f. below).

The explanations provided for the curves (a) – (e) are clearly not unique. If the effects of heating due to filament damage or tunnelling across cracks are introduced for example, one can relatively easily provide a different explanation for any of the *V-I* traces. It is sometimes useful to reverse the direction of current flow and remeasure the sample, because one can distinguish resistive voltages that are current polarity dependent, from thermal voltages that are not. However, one has to be careful that the reversal of the Lorentz force that occurs when the current polarity is reversed, does not damage the (unsupported) sample. The most important point the reader should note here from these data is that one can misinterpret curves (a), (c) and (e), which do not show the intrinsic properties of the conductor, for curves (b) and (d) which are intrinsic. From the *V-I* trace alone, it

may not be possible to reliably distinguish between flux creep (intrinsic to the conductor) and current-transfer (and heating), which can occur because of damage or poor measuring technique. It is concluded that it is essential to employ good practice in mounting samples and is preferable that more than one length of the conductor is measured to ensure the reliability of the results.

The shape or functional form of the *V-I* (or *E-J*) characteristic of a conductor is a complex issue that depends on the details of how the flux is pinned in the superconductor. For technological applications, one uses an empirical parameterisation of the form

$$E = \alpha J^n, \tag{5}$$

or less frequently

$$E = E_0 \exp\left(\frac{J - J_0}{J_E}\right), \tag{6}$$

where α, E_0, n, J_0 and J_E are all experimental or materials constants. The *n*-value is often called the order of transition or index. It is important to note that *n* characterises the entire conducting path between the voltage taps, including the stabilising material. If the conductor is mounted on a metallic (low resistance) sample holder, although current sharing through the shunt may only affect J_c slightly (depending on the criterion used), the value of *n* can decrease significantly (Itoh, Tanaka et al., 1996). High *n* values tend to signify more homogeneous superconductors. Typical values for *n* are between 10 and 100 and in engineering applications tend to be used as a figure of merit.

The *n*-value characterises the sharpness of the *E-J* transition in technological superconductors (Hampshire and Jones, 1985; Hampshire and Jones, 1987a; Bruzzone, 2004); the sharper the transition, the larger the *n*-value (Warnes and Larbalestier, 1986a). The origin of the *n*-value in superconducting wires can be attributed to the distributions in the critical current and the flux-flow resistivity within the filaments (Baixeras and Fournet, 1967; Hampshire and Jones, 1985; Warnes and Larbalestier, 1986a; Warnes and Larbalestier, 1986b; Hampshire and Jones, 1987a; Warnes,

1988; Edelman and Larbalestier, 1993; Wördenweber, 1998). In some simple cases, non-uniformity of the filaments can be the most important factor that determines the *n*-value (Taylor, Keys et al., 2002), in others intrinsic effects are important (Wördenweber, 1998). Experimentally, we have found that the *n*-value approaches 1 as I_c tends to zero for all strands measured – and that this occurs for values of resistivity that are far below the normal state resistivity of either the superconducting filaments or even the copper stabiliser in the strands. This result together with the similar inverted quasi-parabolic strain dependence observed for both the *n*-value and J_c provided the motivation to describe *n* empirically using (Taylor and Hampshire, 2005a)

$$n - 1 = rJ_C{}^s, \tag{7}$$

where r and s are constants and s is typically ~ 0.4 (Taylor and Hampshire, 2005a; Lu, Taylor et al., 2008; Lu and Hampshire, 2009, 2010). However, we have found that strands with almost identical critical current density can have very different *n*-values which suggests that J_c is not always uniquely correlated with *n*, but may also depend on how the current leaves and re-enters a filament to by-pass a region of low J_c. We conclude that detailed understanding of the connectivity between the superconducting regions and the low-resistivity normal regions is still required to provide further insight into *n*-values.

G2.3.4.2 The functional form of the E-J characteristic

For conductors at low temperature, where thermal activation is not important and all the fluxons are moving across the sample or a fixed fraction of the flux is moving across the sample, the *E-J* transition of a superconductor can be described by (Baixeras and Fournet, 1967)

$$E(J) = \rho \int_o^J (J - J_i) f(J_i) d J_i, \tag{8}$$

where J_i is the local critical current, $f(J_i)$ is the distribution of critical currents in the sample, and ρ is the resistivity describing flux flow in regions of the superconductor where the current exceeds the

local critical current. In the analysis, the current density terms represent the current density flowing in the superconductor and therefore, current flowing in the shunt and the stabilising material of the conductor must be subtracted to obtain the correct $f(J_i)$ function (Willen, Zhu et al., 1997). This has been done by measuring the *V-I* characteristic above $B_{c2}(T)$ (Hampshire and Jones, 1985). For high temperature superconductors (HTS), this can be achieved by etching off the matrix (Willen, Zhu et al., 1997; Cai, Polyanskii et al., 1998). By invoking the central limit theorem, it can be assumed that $f(J_i)$ can be described by a normal distribution of the form

$$f(J_i) = \frac{1}{\sqrt{2\pi}}\frac{\beta}{\bar{J}_c}\exp\left\{-\frac{1}{2}\left[\beta\left(\frac{J_i - \bar{J}_c}{\bar{J}_c}\right)\right]^2\right\}, \tag{9}$$

where $\bar{J}_c$ is the average J_c of the distribution, $\sigma(J_i)$ is the standard deviation of the critical current distribution and $\beta = \bar{J_C}/\sigma(J_i)$ (Baixeras and Fournet, 1967; Hampshire and Jones, 1985). Good agreement is found between experimental data and Eqs. (8) and (9). Detailed variable temperature, variable field measurements have been completed on NbTi (Hampshire and Jones, 1985; Hampshire and Jones, 1987a), Nb_3Sn (Hampshire and Jones, 1987b) and V_3Ga (Hampshire, Clark et al., 1989) conductors and scaling laws found for ρ, β, n and $\bar{J}_c$. Equating the empirical equation [Eq. (5)] to the more physical one [Eq. (9)] at $J = \bar{J}_c$ (Hampshire and Jones, 1987a) gives

$$\beta = n\left(\frac{2}{\pi}\right)^{1/2}. \tag{10}$$

This equation is consistent with the empirical finding that homogeneous materials have high values of n (it is not valid for very low n values ($n < 5$) at low E-fields (Edelman and Larbalestier, 1993; Ryan, 1997)). The distribution of critical current densities can be derived explicitly making no assumption about the form of the distribution using (Warnes and Larbalestier, 1986a; Edelman and Larbalestier, 1993)

$$f(J_i) = \frac{1}{\rho}\left(\frac{d^2E}{dJ^2}\right). \quad (11)$$

A graphical representation of this analysis is shown in Figure 9. However, the distribution obtained is sensitive to noise and the algorithm used to calculate the second derivative (Goodrich, Srivastava et al., 1992). It is difficult to measure the distribution at high current because of heating and the local hot spots that occur at high *E*-field values. This is particularly problematic if the stabilising material is etched out of the conductor (Willen, Zhu et al., 1997).

Generalised scaling laws have been developed (Yamafuji and Kiss, 1997) for superconductors operating at high temperatures, where thermal activation and flux pinning can both operate. In some special cases detailed *E-J* characteristics have been calculated, including the formulism for the vortex glass – vortex liquid phase transition in weak-pinning high-T_c superconductors. In general, any realistic mathematical framework is more complex at high temperatures than at low temperatures and a distribution in T_c and $B_{c2}(T)$ will also play a role. Scaling in the *E-J* characteristics has been observed in both low temperature (Cheggour and Hampshire, 1997) and high temperature superconductors (Yamafuji and Kiss, 1997).

Hence for all superconductors, for technological applications, we can use the empirical approach described using Eqs. (5) and (7). If one wants to understand and parameterise the underlying mechanism, at low fields and temperatures, one often finds that J_c is high and thermal activation may play little role. In these cases, sausaging in the conductor filaments, variations in microstructure and composition can be important and one can expect the resultant distribution in J_c to be described using Eq. (9). Alternatively, at the highest fields and temperatures, the distribution in fundamental properties, thermal activation, percolation and regions of very low J_c may dominate the properties of the conductor. In this case the phase transition formalism is probably most appropriate. These two formalisms are still both being developed to better understand and optimise the distribution and magnitude of J_c in conductors.

G2.3.4.3 Magnetic field and temperature corrections to I_c and n-values

In addition to the applied field, there are magnetic field corrections associated with the self-field generated by the sample, by the return current leads, as well as a field correction ($\Delta B_{\mathrm{offset}}$) if the voltage taps are not in field centre on the axis of the magnet bore (associated with the inhomogeneity of the magnet). To first order, the self-field contribution from a straight conductor with current flowing orthogonal to the direction of the applied field is antisymmetric and hence in high fields averages to zero. The self-field correction orthogonal to the direction of the applied field, for example, from the return current in the probe, must be added in quadrature to the applied field, so is also rather small. Hence usually, the difference between the average magnetic field along the wire between the voltage taps and the nominal applied field ($\Delta B_{\mathrm{average}}$)is usually the most important field correction required for technological measurements. Thereafter one can for example use Eq. (4) (or those given later in this article) where the values of $\frac{1}{I_{\mathrm{c}}}\left(\frac{\partial I_{\mathrm{c}}}{\partial B}\right)_T$ are calcuated as a function of field from the scaling law, and the field correction to I_{c} is then

$$\partial I_{\mathrm{c}}(B) = \left(\frac{\partial I_{\mathrm{c}}}{\partial B}\right)_T \left(\Delta B_{\mathrm{average}}\right). \tag{12}$$

For the field correction to the *n*-values ($\partial n(B)$), the value of $\frac{\partial n}{\partial I_{\mathrm{c}}}$ is taken from Eq. (5) and the correction for the *n*-value is given by

$$\partial n(B) = \left(\frac{\partial n}{\partial I_{\mathrm{c}}}\right)_T \left(\partial I_{\mathrm{c}}(B)\right), \tag{13}$$

Temperature corrections can also be required, associated with the helium bath being at a different temperature (ΔT) to 'standard boiling point of helium'. The temperature corrections to I_c and n are simply obtained from Eqs. (12) and (13) after the variables B and T are cycled.

G2.3.5 Case Studies for Testing Different Materials

This section has two parts. The first part surveys some of the most common/important types of measurements reported in the literature. The second part considers specific issues associated for measuring NbTi, Nb_3Sn, BiSCCO and RE-123 conductors. All of these materials either have been or are currently part of international collaborative studies for the standardisation of measurement techniques. The typical errors found when measuring each material are also discussed.

G2.3.5.1 Different types of measurement

I_c as a function of field in liquid cryogens - $J_c(B)$ techniques

Very accurate and stable temperature control can be achieved when making critical current measurements by direct immersion of the conductor in a liquid cryogen, which makes this a popular approach for standard fixed-temperature measurements. However, there are some general points to be aware of when making such measurements.

The vapour pressure of the gas above the cryogenic liquid can be monitored to give the temperature of the bath as suggested by the VAMAS Technical Working Party in their standard method for I_c determination of Nb_3Sn wires (1995). Bath temperatures can be determined from standard tables (2012). In Durham, we have found that UK Government barometric data for weather predictions from local weather stations provide a reliable source of pressure measurements . Temperature errors can occur when using liquid nitrogen if air (primarily oxygen) has dissolved in the nitrogen due to associated changes in the vapour pressure – temperature relation. If atmospheric pressure is used, care must be taken that there is not a build-up of pressure in the Dewar as the critical current transition is reached. Indeed, for very accurate measurements, we use bubblers rather than mechanical valves for helium exhaust as shown in Figure 3. It is prudent to monitor the temperature of the sample during the *V-I* measurement to ensure there is no heating. The type of thermometer used should be chosen based on its properties in high magnetic field (although

magnetoresistance is not a concern per se because we are looking for a constant reading during the measurement rather than absolute values), its sensitivity, and its response time.

In the coil geometry, metal (Ti-alloy (Ridgeon, Raine et al., 2017) and Cu-Be (Cheggour and Hampshire, 2000)) and glass fibre reinforced plastics/epoxy (FRP) are commonly used for the sample holder (c.f. Figure 6). It is common practice that: the wire is wound on to a spirally grooved sample holder to help prevent it from moving during the measurement; the spiral groove should be at an angle no more than 7° to reduce the effects of placing the sample at an angle to the applied magnetic field; copper ends are usually fitted to the sample holder and act as current contacts to which the ends of the sample are soldered and the direction of the Lorentz force is inwards. The groove should preferably be of V-cross-section with a depth approximately equal to the diameter of the wire although thin-walled sample holders should also be grooved to guide the wire (1995). An important consideration when using metallic sample holders is the current sharing that occurs in the dissipative state. Current sharing can produce a large reduction in the *n*-value particularly if a solder bond is used (Itoh, Tanaka et al., 1996). For standard testing of commercial wires for engineering purposes, current sharing is best avoided by using either Ti-alloy or FRP. However, although the technologically important J_e may not be accurately measurable on soldered metallic sample holders, in more fundamental studies that require J_c for the superconducting layer alone, even the current sharing through the stabilising matrix within the conductor itself should be subtracted from the measured data. In such experiments one can use soldered metallic sample holders and treat current sharing through the normal shunt and stabilising material as a single path in parallel with the superconductor. Indeed, in such studies it has been found useful to electroplate a very thin copper layer onto the Ti-alloy sample holder to ease the soldering process, prevent unstabilised conductors from burning out and ensure that localised damaged sections of the wire do not quench the entire conductor during testing. However, electroplating Ti-alloys usually includes using HF acid which requires additional health and safety considerations (Muriale, Lee et al., 1996). The FRP sample

holders should be machined from plate stock so the axis of the tube/cylinder is along the normal direction of the FRP plate. It is less preferred to use rolled FRP tubes with the axis of the tube in "fill" direction because the thermal contraction is more anisotropic than with machined plate and depends on the dimensions on the tube (Goodrich, Bray et al., 1990).

When using solder, in particular for attaching voltage taps, it is important not to thermally shock the conductor. For brittle superconductors, a hot-air gun may be used to warm the conductor uniformly to just below the melting point of the solder before using the soldering iron to attach leads. The temperature of the gun can be set using a thermocouple-based thermometer. Low temperature solder such as $In_{0.52}Sn_{0.48}$ (M.P. ~ 118 °C) can be used to minimise thermal shock (Wiejaczka and Goodrich, 1997; Tsui, Surrey et al., 2016). It should also be noted that standard PbSn solder (M.P. ~ 190 °C) is superconducting at 4.2 K up to ~ 0.1 T.

In low fields I_c can be strongly dependent on whether the applied field has been increased or decreased to obtain the required value i.e. I_c is history dependent (Küpfer and Gey, 1977; Marti, Grasso et al., 1997; Goodrich, 1999/2000). One way to mitigate this problem is to reproduce the magnetic behavior of the application the sample is intended to be used in. If this is not possible, then the dependence of I_c on magnetic field sweep rate and direction should be measured.

In general, one tries to match the thermal contraction of the sample holder to that of the conductor. The properties of any conductor are determined by all its component parts. The sample holders suggested by the standards testing community have been chosen as appropriate for a reasonable range of the common commercial conductors.

$J_c(B,T)$ *experimental techniques*

The variation of critical current as a function of both field and temperature is critical in assessing conductors for cryogen-free applications and for many large-scale systems for which forced flow helium is used. Over limited temperature ranges, vapour pressure thermometry is best used. With

liquid helium, it is possible to vary the temperature between ~ 1.8 K and 5.22 K and with nitrogen from about 55 K to about 85 K. The temperature of the liquid is varied by either decreasing (pumping) or increasing (pressurising) the vapour pressure above the liquid.

Techniques have also been developed to measure conductors in an isothermal environment so the temperature can be varied continuously over any temperature range above 1.8 K (Frost, Jones et al., 1992; Friend and Hampshire, 1995). Typically, the sample is in intimate contact with a copper thermal block that incorporates a heater and thermometry. A temperature controller maintains the temperature constant as the *V-I* characteristics are measured. Purpose built and commercial variable temperature cryostats can also provide the required isothermal environment. Both d.c. continuous and pulsed methods have been used to obtain the *V-I* characteristics (Goodrich, Medina et al., 1998; Kuroda, Murakami et al., 1998).

$J_c(B, T, \varepsilon)$ *experimental techniques*

Although the popular press, and funding agencies, usually consider room temperature superconductivity as the holy grail in applied superconductivity, it is very probable that a new LTS superconducting material (say $T_c = 10$ K) with high J_c and high upper critical field (say J_c = 10^4 A mm^{-2} at 4.2 K and 30 T) that was ductile, would have a larger impact on the development of new markets for superconducting applications. At present all superconductors that are used to produce fields significantly above 10 T are brittle. Hence in these materials, the effect of applied strain on critical current is of great interest, especially for high field applications where the wires are subject to large Lorentz forces (Branch, Tsui et al., 2019).

Historically the short straight geometry (Ekin, 1980; Kamata, Suzuki et al., 1992) was first used to measure the effect of tensile uniaxial strain at 4.2 K on LTS. In order to apply compressive uniaxial strain the sample needs to be supported. Broadly there are two different types of bending springs used for this purpose (c.f. Figure 7). A U-shaped bending spring (in a vertical magnet system) has

been used (ten Haken, 1994) to which a flat-bottomed type hairpin sample can be soldered. Compression or extension is applied to the spring by means of a force applied to its legs which either separates them or brings them together. Strain is measured by a strain gauge either mounted directly on the sample, or in close proximity on the spring. More recently this design has been adapted for measurements on long straight samples in split pair magnets in order to overcome the problems of current-transfer (Fukutsuka, Horiuchi et al., 1984) and to facilitate more accurate measurements on anisotropic materials. Alternatively a helical bending spring can be used which accepts coil type samples (Walters, Davidson et al., 1986). One end of the spring has a torque applied to it whilst the other is held fixed. This mechanism can apply either tension or compression to the sample. In general, variable temperature measurements are made by placing the bending spring in an isothermal environment (Cheggour and Hampshire, 1999; ten Haken, Godeke et al., 1999). Measurements on a range of springs (bending beams) made of different materials has demonstrated that results can be obtained that are independent of the spring material (Taylor and Hampshire, 2005c). In the last 10 years or so, detailed variable-temperature, variable-strain measurements have been completed on a wide range of conductors including Nb_3Sn (Ekin, 1980), Nb_3Al (Takeuchi, Iijima et al., 1997), $PbMo_6S_8$ (Goldacker, Specking et al., 1989), BiSCCO (Ekin, Finnemore et al., 1992; Goldacker, Keßler et al., 1995; Richens, Jones et al., 1997) and RE-123. Typical data are shown in Figure 11 (Keys, Koizumi et al., 2002).

The effect of transverse stress and strain on critical current has also been measured (Ekin, 1987; Kamata, Suzuki et al., 1992; ten Kate, Weijers et al., 1992; ten Haken, 1994). In the earliest work varying stress, samples were placed between a fixed position pressure block and a movable pressure block. The stress is applied by compressing the sample. Although it is not possible to measure the strain in this configuration, it is possible to obtain equivalent stresses for uniaxial strains to allow direct comparison between measurements. The *V-I* characteristics are measured at a series of different stresses. It has been demonstrated that the effect of transverse stress is critically dependent

on how the stress is applied. If the stress is localised, the effect on J_c is far more marked than if the stress is uniformly applied. This can be seen by comparing the degradation of J_c between round and flat conductors (Ekin, 1987; Jakob, Pasztor et al., 1991).There are some limited transverse strain measurements of critical current using samples being developed for this purpose as shown in Figure 7 (Hampshire, 2017).

Critical current measurements have also been performed as a function of stress to estimate the strength of a conductor. In this case the sample was loaded to a certain stress level and then unloaded to zero stress at room temperature. The conductor was then cooled to 4.2 K and the critical current was measured. The variation of critical current as a function of repeated applied stress at room temperature has been measured and the strength distribution for the composite calculated (Ochiai, Osamura et al., 1993).

Pulsed methods for I_c measurements

The most common pulsed method involves increasing the current from zero to a predetermined level in 1-10 ms, measuring the voltage drop along the conductor and ramping back to zero again. The voltage is also measured before and after the pulse to allow for the subtraction of any offset. A series of pulsed measurements can be used to construct the superconducting *V-I* characteristics (Goodrich and Srivastava, 1992). Highly sensitive instruments with rapid response times are required for these measurements. An important advantage of the pulsed method is that if the current contacts are poor (highly resistive), they have limited effect on the measurement because there is not sufficient time during the pulse for the heat to diffuse to the part of the conductor between the voltage taps. Measurements have also been performed using pulsed magnetic fields (Hole, 1995). In this case, a constant current is applied to the sample, and the voltage generated is recorded. This method has the advantage of allowing measurements to be taken up to the highest fields (>50 T). The rapid change

in magnetic field, however, causes eddy current heating that can prevent accurate measurements on some samples.

Persistent mode experiments

The *V-I* characteristics at very low electric fields can be found by measuring the decay of the current in a persistent mode coil (Ryan, Jones et al., 1997). A current is induced into a superconducting coil, and the decay of the self-field measured a function of time. The decay can be converted into an equivalent resistance for the conductor. This is presently the only method which gives measurements on long lengths of conductor down to an electric field of a few pV m^{-1} relevant for NMR applications. Results obtained on NbTi and Nb_3Sn are in broad agreement with a normal distribution of critical currents described using Eqs. (9) and (10).

G2.3.5.2 Measurements on specific materials

In this second part, we first consider know-how accrued in the community that is relevant for measuring different types of materials. The approach for measuring a ductile superconductor such as NbTi can be different to that for measuring a brittle RE-123 HTS tape. For each material we also consider how we parameterise $J_c(B,T,\varepsilon)$ data. There are a number of different approaches in the literature. We have not chosen to try to outline them all here, but rather describe the most complete approach that we favour but also point to other literature. It is understandable that there are different approaches because there are competing issues; in Durham we tend to analyse comprehensive $J_c(B,T,\varepsilon)$ datasets that include the full range of operation for the material. Such data is usually very hard-earned so we tend to parameterise the data knowing that parameterisation will be interrogated using interpolation. Some of the data in the literature can be more limited, and quite reasonably the authors are more concerned about parameterisations that include extrapolation (Ekin, Cheggour et

al., 2016). This field is important, dynamic and vibrant. We point to some of the open questions and research at the end.

NbTi

NbTi is probably the most important technological superconductor. It is a ductile material with a high upper critical field and hence the material of choice for most MRI applications up to about 10 T. It is usually measured using the coil geometry. The insulation on most technological NbTi wires can be removed mechanically using emery paper or chemically using a mixture of phenol/methylene chloride to prevent mechanical damage during sample preparation. Both Ti-alloy and FRP are often used for the measurement barrel. In Durham we routinely use Ti-alloy barrels for measuring NbTi as shown in Figure 6. The FRP used is G-11CR (US notation) or EP GC 203 (European notation) which has a thermal contraction similar to NbTi. If the sample is held in place using varnish, a strong epoxy (such as Stycast), vacuum grease, or no bond at all, there is little effect on I_c (Goodrich and Srivastava, 1995a). The critical current values for samples on a Ti-alloy sample holder are similar to values from samples mounted on G10 (Ogawa, Kubo et al., 1996).

One of the "standard measurements" laboratories in the USA (NBS/NIST) has produced a standard reference NbTi material (SRM 1457) that has been tested for long length homogeneity and measured extensively in interlaboratory comparisons. There is now routinely excellent agreement between laboratories measuring NbTi. Critical currents were measured at 2, 4, 6 and 8 T on FRP for temperatures from 3.90 K to 4.24 K using electric field criteria from 5 to 20 $\mu V\,m^{-1}$. The total uncertainty of the reported critical current values at any of the four magnetic fields was no greater than 2.6% (Goodrich, Vecchia et al., 1984). In subsequent series of measurements, the uncertainties for the critical currents (measured at an electric field criteria of 10 $\mu V\,m^{-1}$) were found to be 1.71% and 1.97%, and the difference between the interlaboratory averages and certified critical currents were 0.2% and 0.3% for 6 and 8 T respectively (Wada, Goodrich et al., 1995). In the IEC/TC90

experiments, the coefficient of variation for samples mounted on FRP (standard deviation divided by the average value) was lower than 2% for I_c measurements from 1 to 7 T (Ogawa, Kubo et al., 1996).

There is only limited variable-strain J_c data in the literature. It shows that NbTi is reasonably insensitive to strain (Goodrich, Vecchia et al., 1984). This insensitivity means that very accurate measurements will be required to characterise the strain dependence comprehensively, that include proper account of: the relatively small changes in B_{c2} that occur for the different criteria used to define B_{c2}; geometrical changes in the sample on applying the strain; and the small anisotropy in B_{c2} associated with the drawing of the wire during fabrication. The strain insensitivity also means that the Ginzburg-Landau parameter is rarely included in the parameterisation of J_c as a function of field and temperature (c.f. Eq. (4)) and is usually taken to be of the form (Friend and Hampshire, 1993)

$$F_P = A[B^*_{c2}]^2 b(1-b), \tag{14}$$

where A is a constant and the effective upper critical field is taken to be of the form

$$B^*_{c2}(T) = B^*_{c2}(0)(1-t^v), \tag{15}$$

where $t = T/T_c$, where T is the temperature and $T_c = 9.45$ K and for the current density orthogonal and parallel to the applied field, $B^*_{c2}(0)$ and v can be taken to be 15.8 T and 1.56 (orthogonal) and 14.9 T and 2.15 (parallel).

Nb_3Sn + Nb_3Al

The large sensitivity of Nb_3Sn and Nb_3Al to mechanical strain means that care must be taken when reacting and mounting samples to avoid degrading J_c prior to measurement. In the past, Nb_3Sn conductors were reacted on a stainless steel reaction mandrel (that had been oxidised), or sometimes a carbon reaction mandrel, of a geometry that closely matched the sample holder. The sample was then carefully transferred on to the sample holder taking care not to unduly strain the wire during this operation. A G10-CR (US notation) (EP GC 201: European notation) which (machined from plate) is similar to G-11CR (used for NbTi), but has a differential thermal contraction better matched to

Nb_3Sn was used (Kirchmayr, Siddall et al., 1995). Other materials with similar thermal expansion properties to Nb_3Sn conductors are non-magnetic stainless steels, copper or non-magnetic copper alloys (see Figure 5) and have also been used. As part of the VAMAS report, similar I_c's as a function of magnetic field were found using G10 and stainless steel sample holders. Vacuum grease was suggested as the bonding agent in the VAMAS test as it is easy to remove from the sample after use. Stycast (a high strength epoxy) was also tested and gave similar I_c's for stainless steel and G10-CR sample holders (Kirchmayr, 1995). The IEC/TC90 round-robin test on Nb_3Sn composite conductors advised explicitly against using a solder bond on the stainless steel. Alumina ceramic, like stainless steel, has also been used as a dual-purpose mandrel/sample holder, either by itself or as a coating on stainless steel (Goodrich and Srivastava, 1995a) because there was less chance of bonding between the holder and the conductor, although the thermal expansion is not very well matched (Wada, Goodrich et al., 1995).

However, following the huge international effort directed at fabricating the toroidal field coils for ITER, a dedicated mandrel based on a very resistive Ti-alloy, as shown in Figure 6, on which the sample can be both reacted and measured has eliminated the need to transfer the sample from the reaction mandrel to the measurement mandrel. As a result, I_c measurements on Nb_3Sn samples typically vary between laboratories by ~ 3% and most of the variation is probably associated with variability in the temperature of the reaction process in the furnaces (Raine, T et al., 2017). In Durham we use the ITER-like barrel for almost all I_c measurements at cryogenic temperatures. For both Nb_3Sn and Nb_3Al measurements, the surface of the reaction mandrel is first heavily oxidized for 3 h at 300 °C in air, to prevent any diffusion bonding between it and the conductor. The wire is then wound on the mandrel for the heat-treatment during which brittle A15 compound is formed. The sample is soldered onto the copper rings and the measurements made. We have found that for both Nb_3Sn (Keys and Hampshire, 2003; Taylor and Hampshire, 2005b) and Nb_3Al (Keys, Koizumi et al., 2002), the volume pinning force density is very approximately given by

$$F_{\mathrm{P}} = J_{\mathrm{c}}B = A\frac{[B_{\mathrm{c2}}^{*}]^{5/2}}{(2\pi\phi_0)^{1/2}\mu_0[\kappa_1^{*}]^2}b^{1/2}(1-b)^2, \tag{16}$$

where A is a dimensionless constant $\sim 1/250$ for Nb_3Sn and $\sim 1/100$ for Nb_3Al. A simple dimensionality energy argument suggests that the equation is reasonable.

Accurate fits to $J_{\mathrm{c}}(B, T = 4{,}2K)$ and $J_{\mathrm{c}}(B, T)$ data using Eq. (4) lead to values for n, m, p and q, that are not always integral and half-integral. This can be attributed to the large distribution of fundamental parameters in this high J_{c} technological material. Incorporating both microscopic (BCS) and phenomenological (GL) theory (Bardeen, Cooper et al., 1957; Helfand and Werthamer, 1966; McMillan, 1968; Allen and Dynes, 1975; Orlando, McNiff et al., 1979; Kresin, Gutfreund et al., 1984; Kresin, 1987; Carbotte, 1990), considering the effects of strong coupling (Keys and Hampshire, 2003) and after some considerable care to look at the correlations been the free-parameters (Keys, Koizumi et al., 2002), we found that when parameterising J_{c}data as a function of magnetic field, temperature and strain, Eq. (4) can be rewritten

$$J_{\mathrm{c}}(B, T, \varepsilon_{\mathrm{I}}) = A(\varepsilon_{\mathrm{I}})\left[T_{\mathrm{c}}^{*}(\varepsilon_{\mathrm{I}})[1-t^2]\right]^{m}[B_{\mathrm{c2}}^{*}(T, \varepsilon_{\mathrm{I}})]^{n-m-1}b^{p-1}[1-b]^{q}, \tag{17}$$

where the superconducting parameters are described using

$$B_{\mathrm{c2}}^{*}(T, \varepsilon_{\mathrm{I}}) = B_{\mathrm{c2}}^{*}(0, \varepsilon_{\mathrm{I}})[1-t^{\nu}], \tag{18}$$

$$\left\{\frac{A(\varepsilon_{\mathrm{I}})}{A(0)}\right\}^{1/u} = \left\{\frac{B_{\mathrm{c2}}^{*}(0, \varepsilon_{\mathrm{I}})}{B_{\mathrm{c2}}^{*}(0{,}0)}\right\}^{1/w} = \left\{\frac{T_{\mathrm{c}}^{*}(\varepsilon_{\mathrm{I}})}{T_{\mathrm{c}}^{*}(0)}\right\}, \tag{19}$$

and

$$\frac{B_{\mathrm{c2}}^{*}(0, \varepsilon_{\mathrm{I}})}{B_{\mathrm{c2}}^{*}(0{,}0)} = 1 + c_2\varepsilon_{\mathrm{I}}^2 + c_3\varepsilon_{\mathrm{I}}^3 + c_4\varepsilon_{\mathrm{I}}^4, \tag{20}$$

where J_{c} is the engineering critical current density and ε_{I} is the intrinsic strain, determined by the applied strain, ε_{A}, and the applied strain at the peak in J_{c}, ε_{M}, according to (Rupp, 1977; Luhman, Suenaga et al., 1978; Markiewicz, 2004a)

$$\varepsilon_{\mathrm{I}} = \varepsilon_{\mathrm{A}} - \varepsilon_{\mathrm{M}}. \tag{21}$$

By making measurements in magnetic fields up to 28 T in the Grenoble High Field Magnet Laboratory on three different Nb_3Sn samples, so that the upper critical fields of the three strands were measured directly over much of the phase space, we concluded that one can fit $J_c(B,T,\varepsilon)$ data for many Nb_3Sn strands using some universal parameters ($n = 2.5$, m= 2, $\nu = 1.5, w = 2.2$, $u = 0, c_2 = -0.77462$, $c_3 = -0.59345$, $c_4 = -0.13925$) and reduce the number of free parameters to 6, namely $A(0)$, $T_c^*(0)$, $B_{c2}^*(0,0)$, p , q and ε_M.

The reader will find many different approaches to parameterising $J_c(B,T,\varepsilon)$ data in the literature (Ekin, Cheggour et al., 2016). Some are motivated by a different utility to the work above, others we feel are not correct. We note that the fitting procedure that we have always used minimises the percentage error between the fits and the data. This has the advantage that the free parameter values obtained do not depend on whether one fits F_P or J_c, which is consistent with the errors in the experiment. Indeed, we recommend that when commercial packages are used to find the free parameters, one checks that they are not dependent on whether one fits F_P or J_c. Tabulations of $J_c(B,T,\varepsilon)$ and n-value data taken in Durham have been made available as well as the scaling-law parameterisation of $J_c(B,T,\varepsilon)$ and $n(B,T,\varepsilon)$ for many Nb_3Sn strands on the Internet (Durham-Superconductivity-Group). The polynomials in Eqs. (17) to (21) were motivated by finding the best fit to the data, although it is clear that there are other options if one intends extrapolating to higher strains than those measured, rather than interpolating. An alternative nine-parameter fit which follows excellent work that explicitly incorporates the 3-dimensional nature of strain into the scaling law (ten Haken, Godeke et al., 1995; Markiewicz, 2004b, a, 2008) has also been suggested. However, unfortunately it effectively includes a $1/\kappa$ term rather than the $1/\kappa^2$ found for example by Dew-Hughes (Dew-Hughes, 1974) and Kramer (Kramer, 1973, 1975).

Multifilamentary BiSCCO – 2212 and 2223 and RE-123.

Because it is often not possible to wind high temperature superconducting tapes into small coils for measurements in small bore magnets without generating a large strain, most interlaboratory comparison measurements on high T_c tapes use the short straight geometry (Wiejaczka and Goodrich, 1997). Some BiSCCO conductors are not fully dense. For the Ag-sheathed BiSCCO tapes and wires, it was observed that the thermal expansion was dependent on thermal cycling, which was attributed to yielding due to an internal stress between the Ag-sheath and the BiSCCO(2223) filaments (Yamada, Nara et al., 1998). Since cryogenic liquid can seep into the conductor during measurements, it is essential to warm the samples slowly after measurement so the cryogen can escape without blistering the silver matrix (Wiejaczka and Goodrich, 1997). Equally the RE-123 samples can delaminate. Hence when measuring either BiSCCO or RE-123, one can mitigate against damage by encapsulating the sample. Brass, G10, Ti-alloy and CuBe have all been used as sample holders. However, it has been reported that BiSCCO samples are more likely to separate from the substrate when mounted on brass (due to differential thermal contraction) which can damage the samples. Hence the samples can be bonded and encapsulated to a G10 sample holder using a glass filled epoxy. One can also use low temperature solder with copper-plated Ti-alloy or CuBe to encapsulate and bond the sample. For all sample holders, current contacts and voltage taps are soldered directly to the sample using a low temperature solder. However, although some damage is likely caused by soldering, successful measurements on short samples have been made by soldering the current leads and using silver paint/epoxy for voltage taps (Sneary, Friend et al., 1999).

For systems analysis, where a rough and simple approximation to the angular dependence is sufficient, we have found J_c of HTS tapes can be roughly described as a function of field (B), temperature (T), angle of the field with respect to the tape (θ) and strain, using (Lee, Jenkins et al., 2015)

$$J_c \approx \alpha(T,\varepsilon)\left(1-\frac{B}{B_{c2}}\right)\exp\left(-\frac{Bcos\theta}{\beta(T)}\right), \quad (22)$$

where the free parameters $c(T)$, and $\beta(T)$ can be taken as functions of temperature alone. Variable strain can also be parametersied using $\alpha(T,\varepsilon)=\alpha(T)\left(1-c(T)\left(\varepsilon-\varepsilon_0(T)\right)^d\right)$ as demonstrated from fits to variable strain J_c data from Sunwong (Sunwong, Higgins et al., 2013) and Sugano (Sugano, Shikimachi et al., 2010). In round robin testing, the coefficient of variation for a BiSCCO sample premounted by a central laboratory (NIST) were 4.4% (77 K) and 3.2% (4.2 K) (Wiejaczka and Goodrich, 1997). The IEC/TC90 has developed a d.c. critical current test method for Ag-sheathed BiSCCO conductors (IEC, 2006b) and a public database of critical current data of HTS conductors is now available for magnet designers (Wimbush and Strickland, 2017).

G2.3.6 Concluding Remarks

The development of reliable techniques for testing conductors is essential for underpinning a mature technology based on superconductivity and a better understanding of the underlying science. In light of the new complex composite conductors that are continuously being developed, the international community is committed to improving the testing of conductors. Domestic and international programmes for laboratory intercomparisons of mechanical, thermal and electromagnetic measurements are in progress. This review has provided an introduction to testing the current carrying capacity of conductors. We hope that it provides a good introductory review for scientists new to such work and helps them with making reliable measurements.

G2.3.7 Acknowledgements

The authors wish to thank the U.K Engineering and Physical Sciences Research Council (EPSRC) and Siemens for their support. The authors thank: Prof. K. Osamura and Dr. L. Goodrich for their help in providing literature for this article; P.A. Russell for her help with producing the figures; and members

of the superconductivity group in Durham particularly A. Blair and P. Branch. Figure 1(a) and 1(b) are courtesy of Dr. B. Mendis and L. Bowen in the Durham University Microscopy Facility. Figure 1(f) is courtesy of SuperPower, Inc., a Furukawa Company, copyright 2015. This work was funded by the RCUK Energy Programme under grant EP/I501045 and EP/L01663X/1. The data are available at: http://dx.doi.org/10.15128/r1pn89d656x

Figures

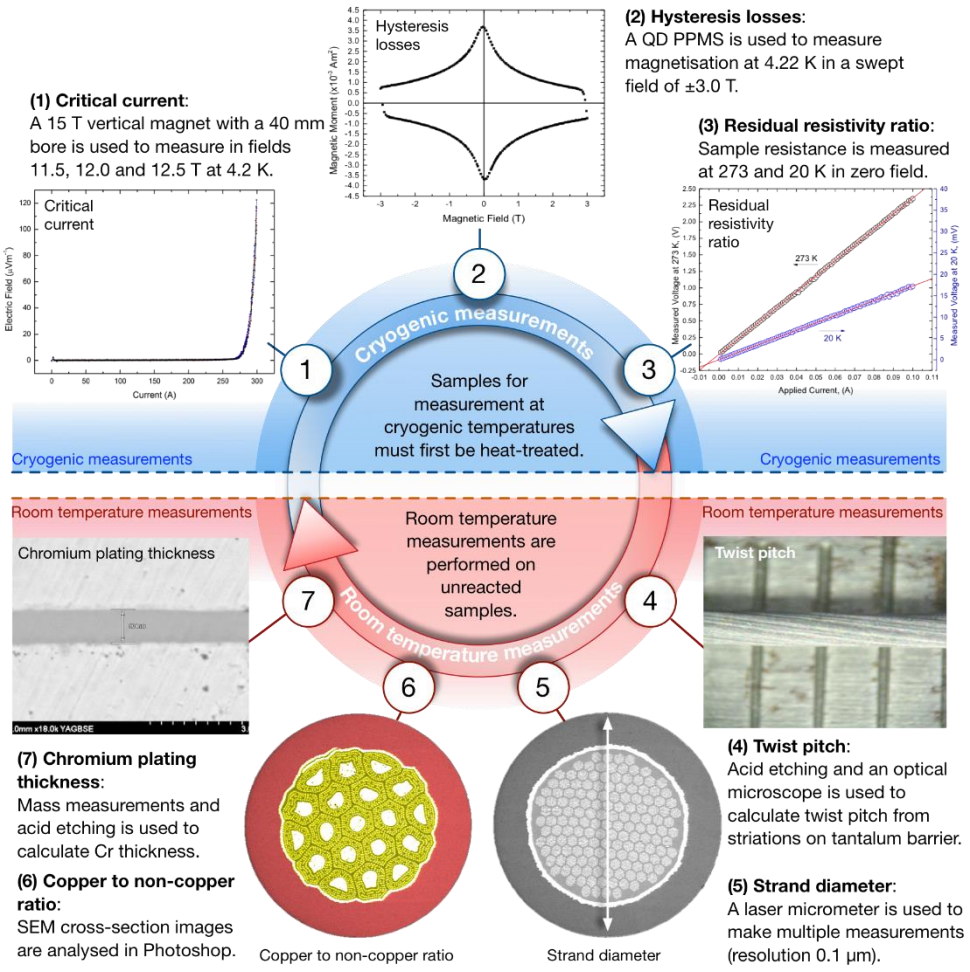

Figure 1: The seven measurements used to characterise the Nb_3Sn strands for ITER's toroidal field coils (Sborchia, Fu et al., 2008). A similar set of measurements, with the inclusion of an additional plating adhesion test, is used to characterise the NbTi strands for ITER's poloidal field coils (Sborchia, Fu et al., 2008). Acid etching cannot be used to remove the nickel plating coating on the NbTi strands so a couloscope is used to perform reverse electrolysis.

a)

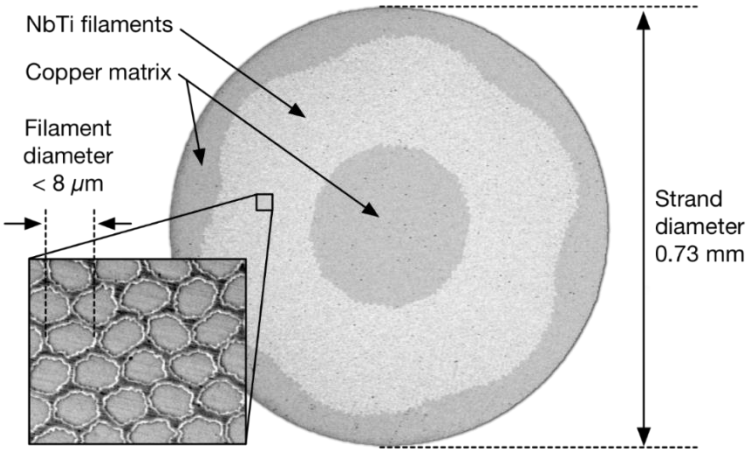
NbTi filaments
Copper matrix
Filament diameter < 8 μm
Strand diameter 0.73 mm

b)

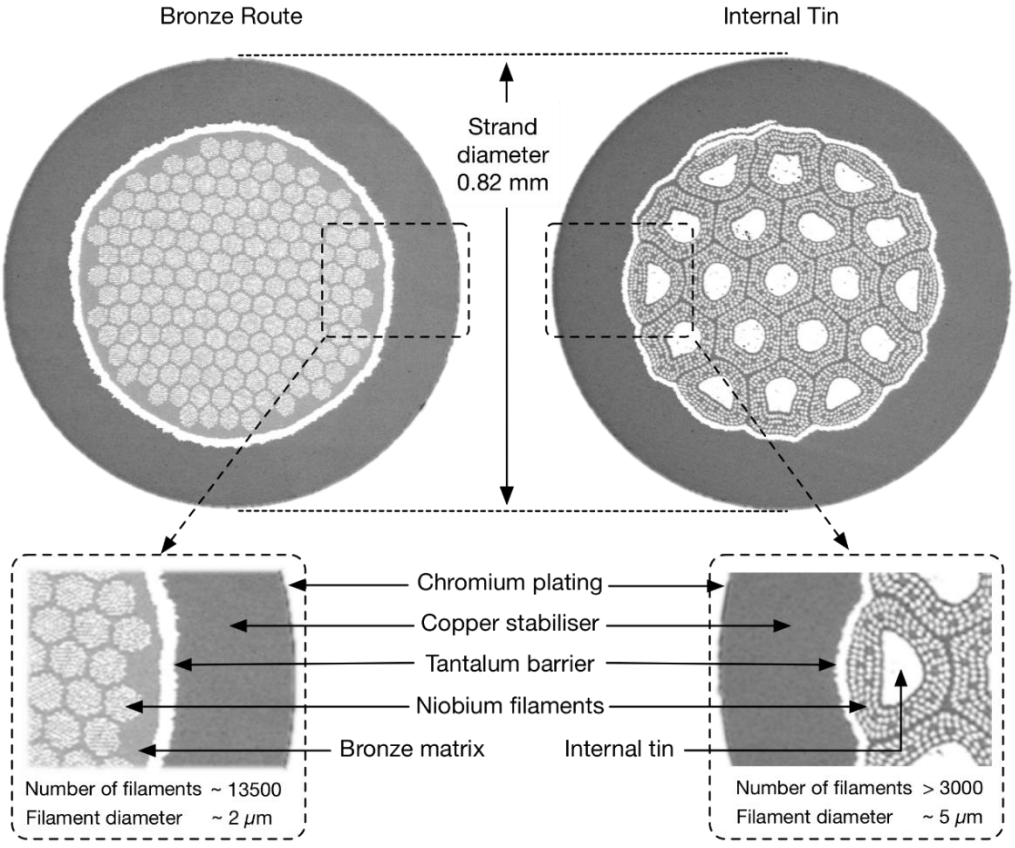
Bronze Route
Internal Tin
Strand diameter 0.82 mm
Chromium plating
Copper stabiliser
Tantalum barrier
Niobium filaments
Bronze matrix
Internal tin
Number of filaments ~ 13500
Filament diameter ~ 2 μm
Number of filaments > 3000
Filament diameter ~ 5 μm

c)

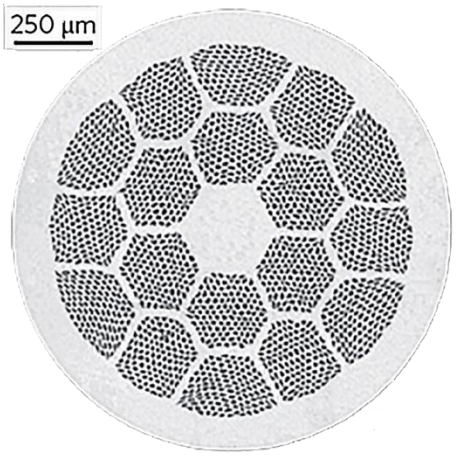

d)

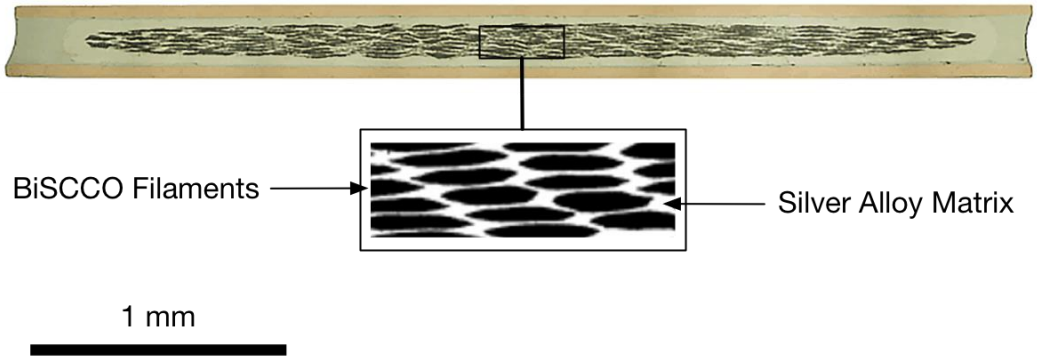

e)

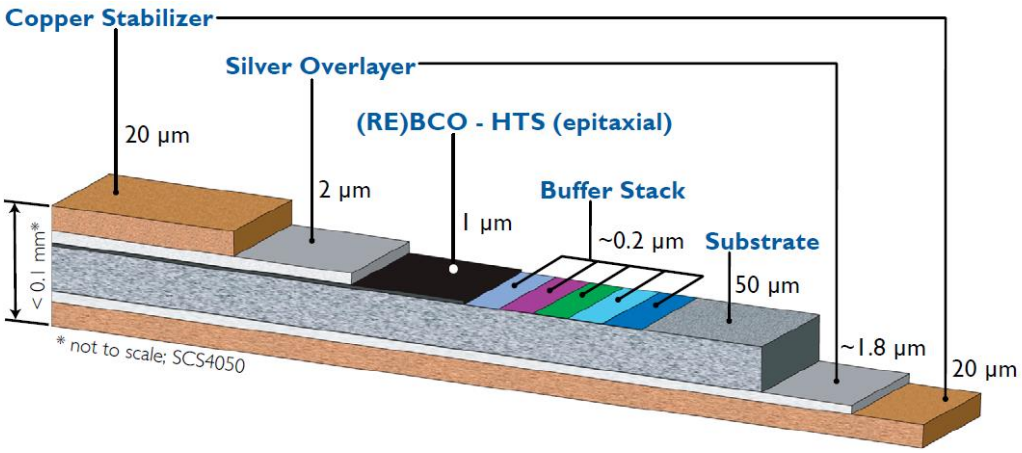

Figure 2: Schematic diagrams of conductors a) Cu-NbTi (inset (Muzzi, De Marzi et al., 2011)), b) Multifilamentary bronze route Nb_3Sn and Modified Jelly Roll Nb_3Sn, c) Ag-sheathed Bi-2212 (Larbalestier, Jiang et al., 2014), d) Bi-2223 (Sato, 2017), and e) Rare-earth-123 (SuperPower-Furukawa, 2013).

a)

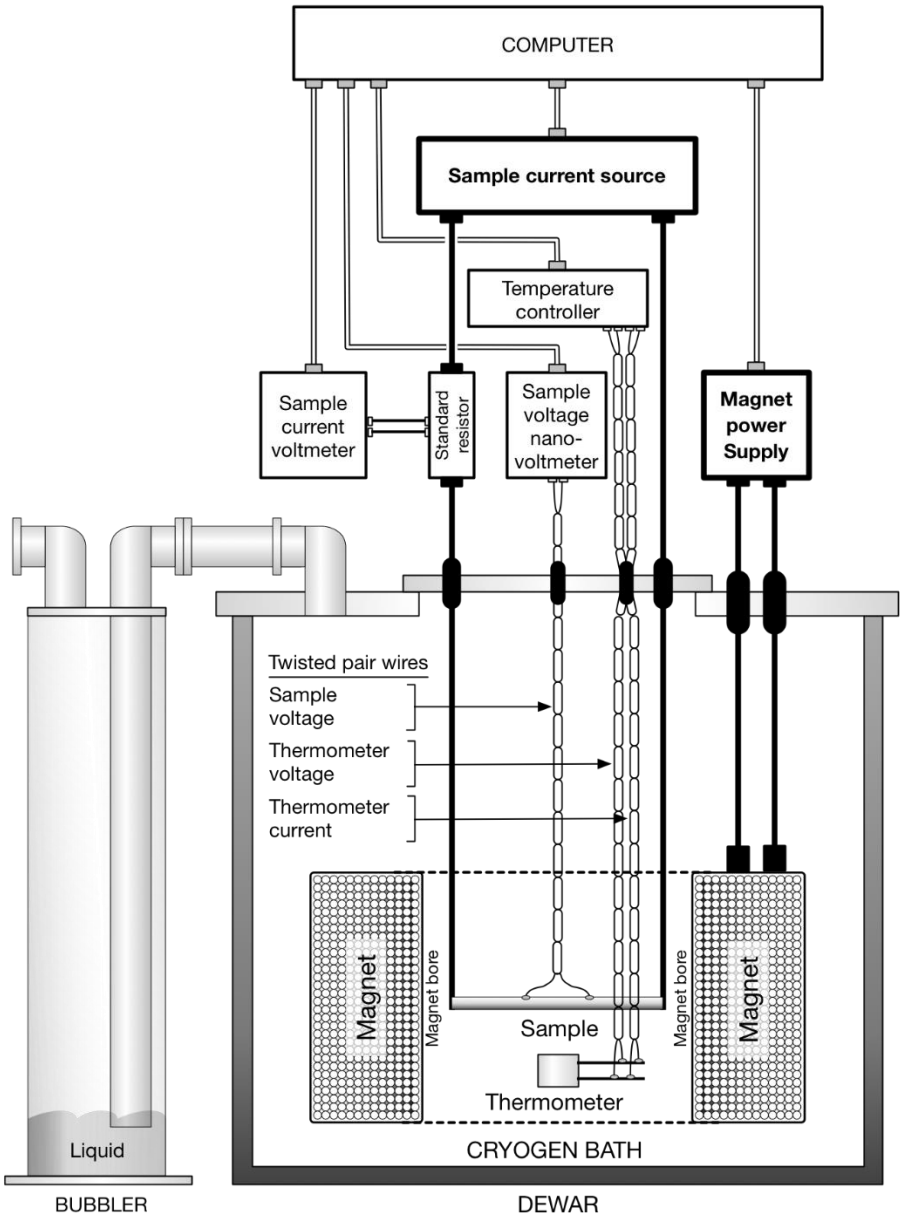
COMPUTER
Sample current source
Temperature controller
Sample current voltmeter
Standard resistor
Sample voltage nano-voltmeter
Magnet power Supply
Twisted pair wires
Sample voltage
Thermometer voltage
Thermometer current
Magnet
Magnet bore
Sample
Thermometer
Magnet bore
Magnet
Liquid
CRYOGEN BATH
BUBBLER
DEWAR

b)

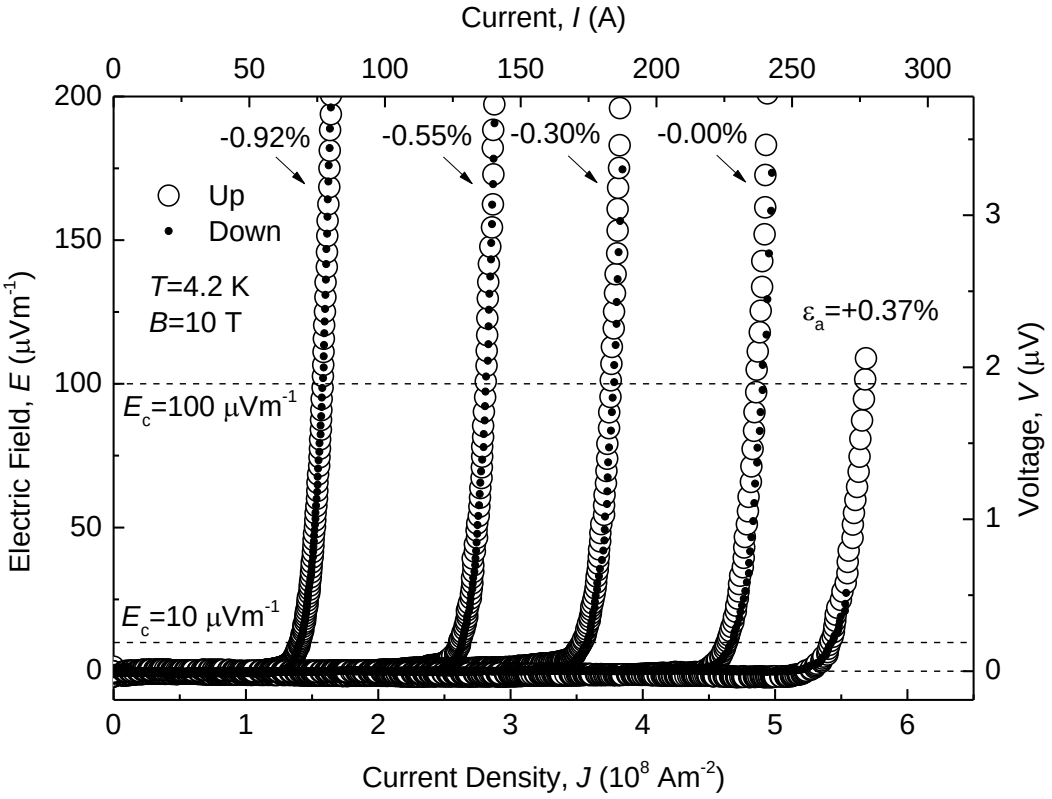

Figure 3: a) A block diagram of equipment for measuring critical current density in strand conductors (the bubbler is used to maintain the liquid helium at close to atmospheric pressure), and b) Typical *E-J* characteristics generated for a Nb_3Sn strand at 4.2 K and 10 T at different values of strain (Tsui and Hampshire, 2012). A 21-point smoothing process has been applied to reduce the noise from the raw data without altering the shape of the transition. Each pair of *E-J* characteristics at a given strain were obtained during the strain cycle from +0.4% down to -1.1% and back up to 0.4 % strain. The figure shows that the *E-J* characteristics are a reversible function of strain over the strain range measured.

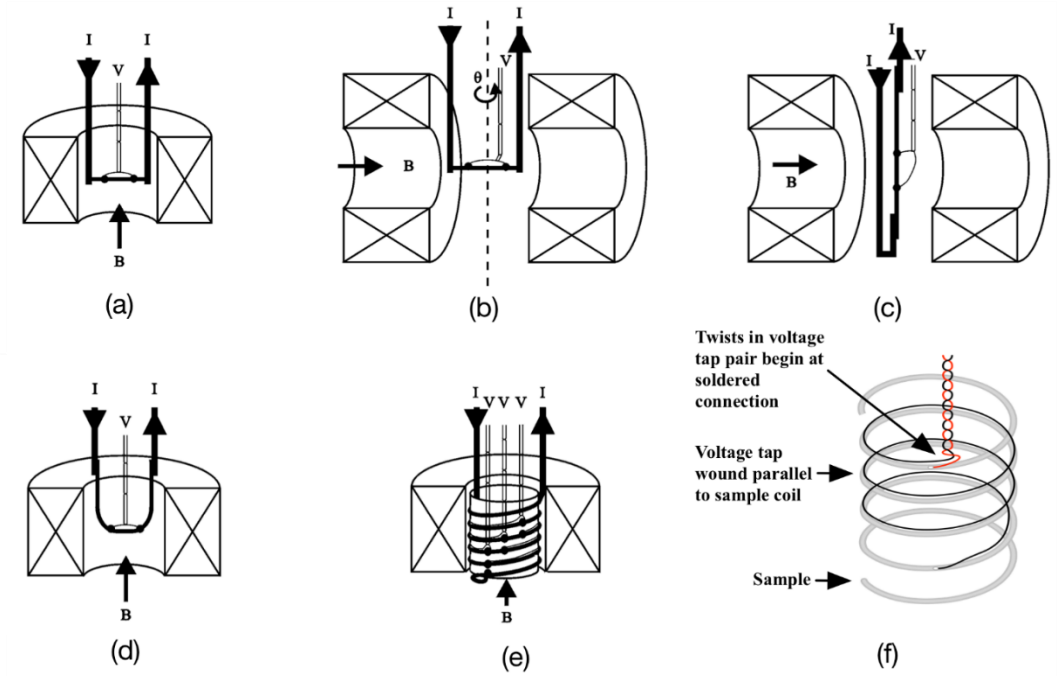

Figure 4: Different geometries for performing critical current measurements. a) Short straight sample measured in a vertical solenoidal magnet, b) Short straight sample for finding the angular dependence of critical current with magnetic field, c) Long straight sample measured in a horizontal split-pair magnet d) Hairpin sample geometry, e) Coil geometry (f) Detail of voltage lead attachment to minimise inductive voltages for the helical geometry.

a)

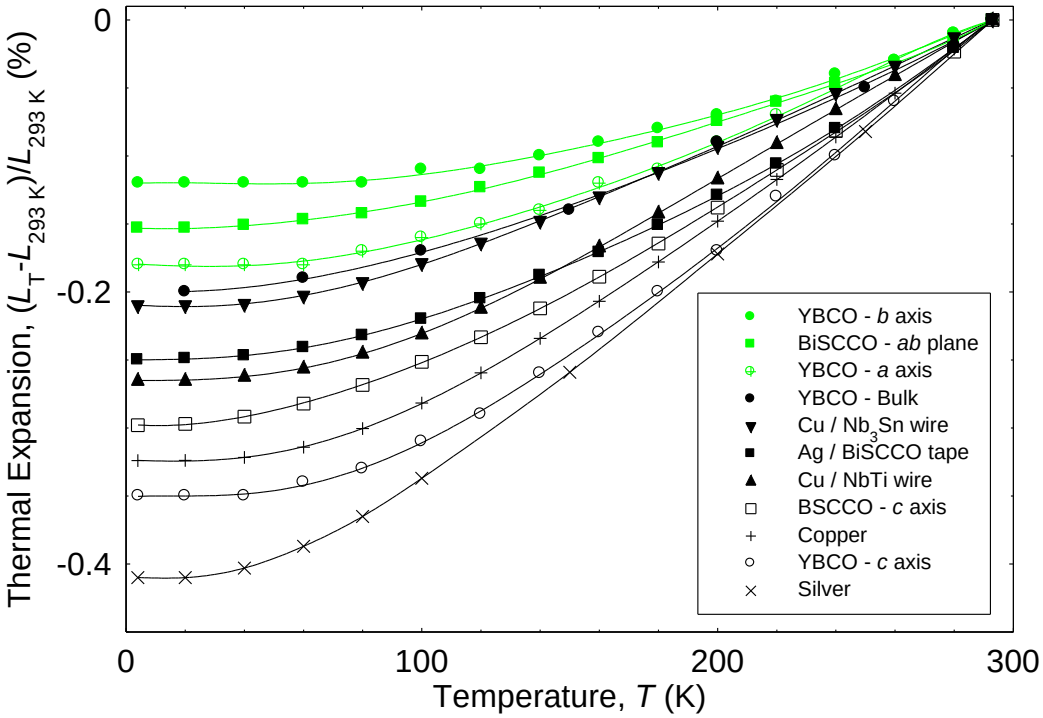
Thermal Expansion, $(L_T-L_{293\ K})/L_{293\ K}$ (%)
0
-0.2
-0.4
0
100
200
300
Temperature, T (K)
YBCO - b axis
BiSCCO - ab plane
YBCO - a axis
YBCO - Bulk
Cu / Nb_3Sn wire
Ag / BiSCCO tape
Cu / NbTi wire
BSCCO - c axis
Copper
YBCO - c axis
Silver

b)

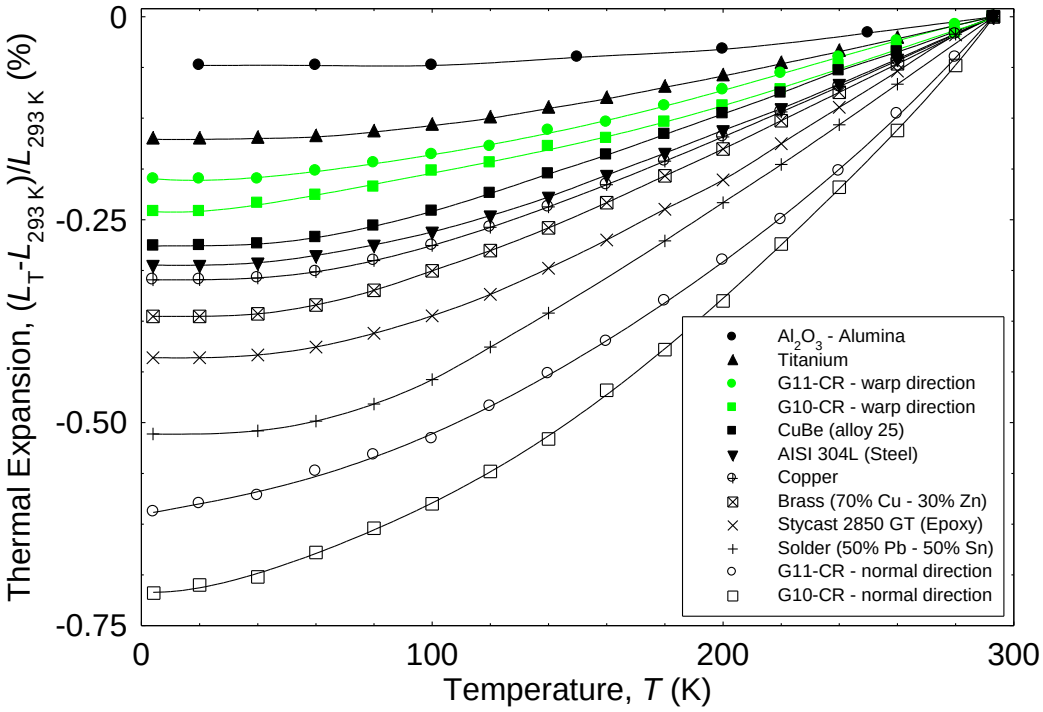
Thermal Expansion, $(L_T-L_{293\ K})/L_{293\ K}$ (%)
0
-0.25
-0.50
-0.75
0
100
200
300
Temperature, T (K)
Al_2O_3 - Alumina
Titanium
G11-CR - warp direction
G10-CR - warp direction
CuBe (alloy 25)
AISI 304L (Steel)
Copper
Brass (70% Cu - 30% Zn)
Stycast 2850 GT (Epoxy)
Solder (50% Pb - 50% Sn)
G11-CR - normal direction
G10-CR - normal direction

Figure 5: Thermal expansion as a function of temperature for a) superconducting compounds, composites and matrix materials (Clark, Fujii et al., 1981; White, 1987; Meingast, Kraut et al., 1991; Okaji, Nara et al., 1994; White, 1998; Yamada, Nara et al., 1998) – the Nb_3Sn conductor includes a tungsten core and b) mandrel materials and bonding agents (Clark, 1983; Pobell, 1996; White, 1998; Cheggour and Hampshire, 2000).

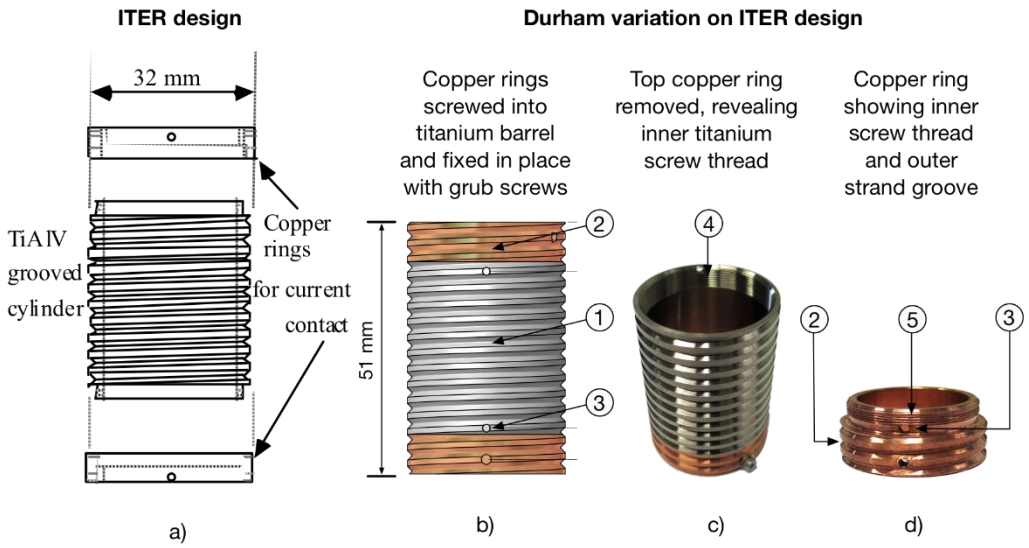

Figure 6: a) The standard ITER barrel design showing the separate top and bottom copper current rings and the central titanium cylinder (Nijhuis, Wessel et al., 2006). Note that only the titanium cylinder is prepared with a groove to support the sample strand. The copper rings are pinned (or supported with screws) onto the titanium cylinder. b) The Durham barrel has copper current rings screwed into the titanium cylinder. Note that the sample strand support groove (1) from the titanium cylinder is extended into the copper rings (2). Grub screws hold the copper and titanium together (3) c) Durham barrel with top copper ring removed showing an internal screw thread (4) for copper ring attachment. d) Copper ring showing the screw thread (5) (for attachment to the titanium cylinder) and the outer sample support groove (2). IN Durham we routinely use this barrel to measure both NbTi and Nb_3Sn strands.

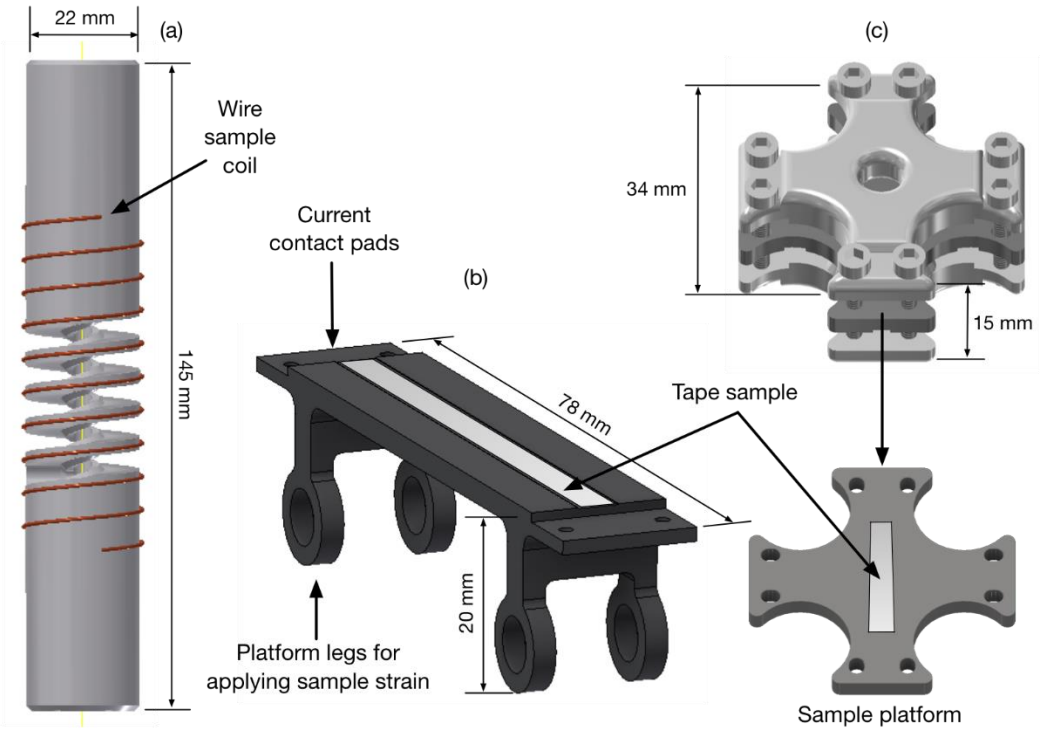

Figure 7: Different geometries for sample holders used to make critical current measurements under applied strain. a) A spring barrel used to make variable-strain I_c measurements in a vertical magnet (Walters, Davidson et al., 1986; Taylor and Hampshire, 2005c), b) a 'spring-board' sample holder used to make variable-strain I_c measurements in a horizontal magnet (Sunwong, Higgins et al., 2013; Sunwong, Higgins et al., 2014) and c) a crossboard for simultaneously applying longitudinal and transverse strains to a sample while making I_c measurements in either a horizontal or vertical magnet (Hampshire, 2017).

a)

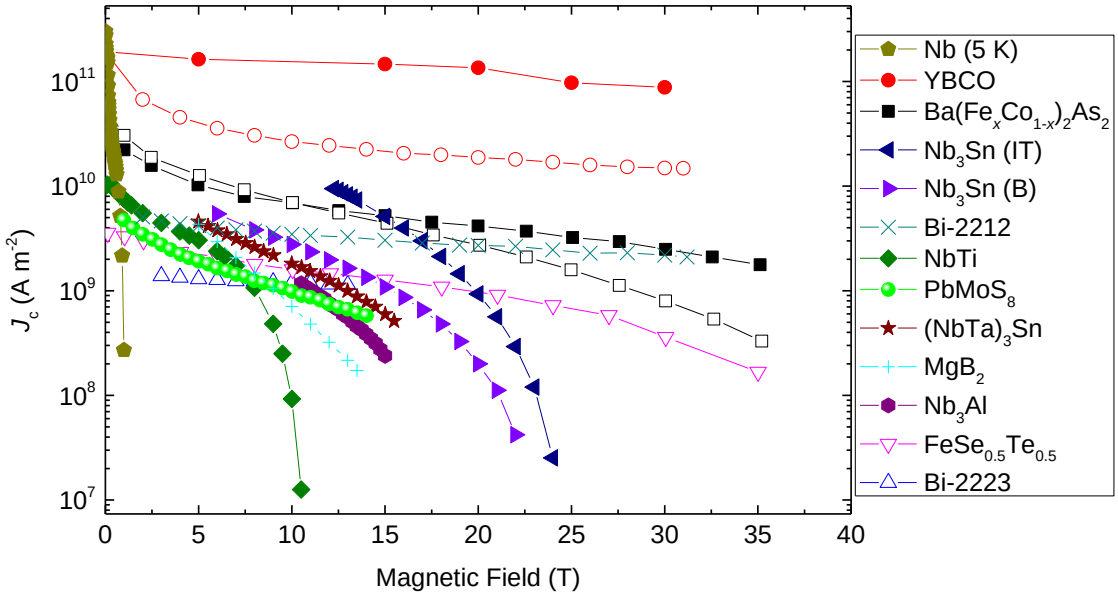

b)

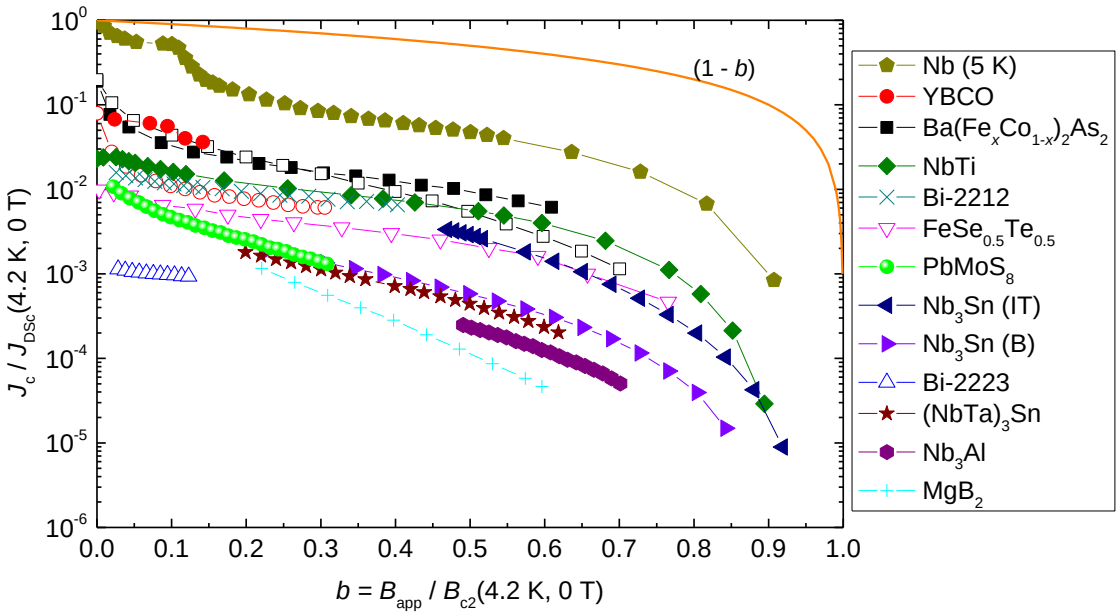

Figure 8: (a) Typical critical current density values in the superconducting layer itself for the most important high-field superconductors (b) Typical critical current density values normalised by the

depairing current density at 4.2 K and zero magnetic field, for the most important high-field superconductors. Closed symbols denote parallel and open symbols perpendicular to the sample plane. The solid red line in the lower panel gives the field dependence of the depairing current derived from Ginzburg-Landau theory. Courtesy of G. Wang *et. al*. (Wang, Raine et al.).

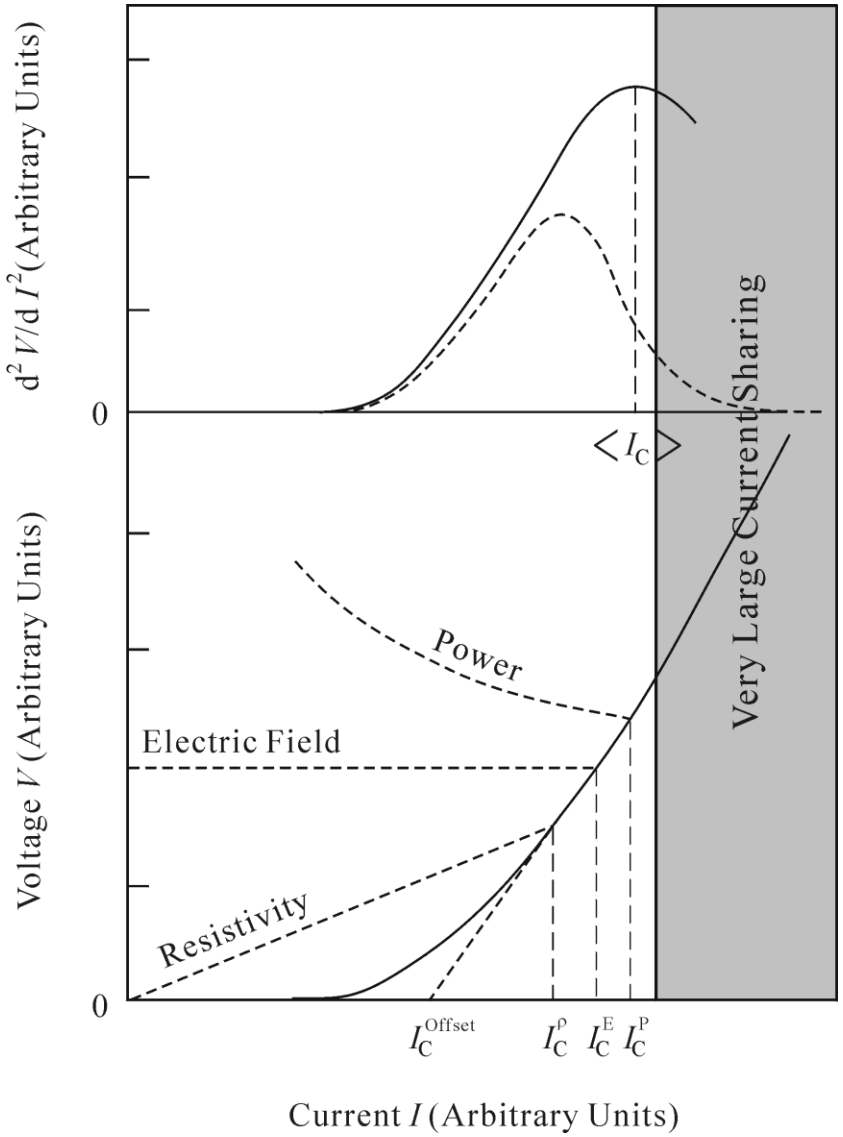

Figure 9: The lower panel shows the conventions used to define I_c – the electric field, resistivity and power criteria as well as the offset method. The upper panel shows d^2V/dI^2. The dotted line is for the

conductor and shunt (Willen, Zhu et al., 1997). The solid line is for the superconductor alone and can be equated to the distribution in I_c.

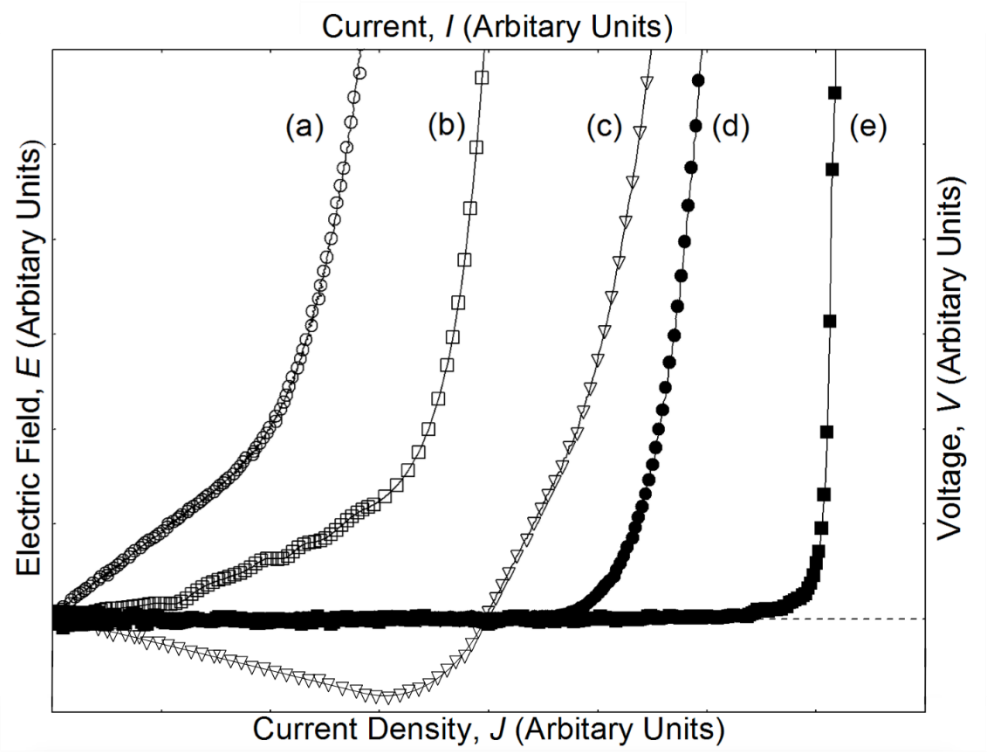

Figure 10: Schematic *V-I* characteristics illustrating (a) current-transfer, (b) flux creep, (c) a thermal voltage followed by current-transfer, (d) flux flow, and (e) thermal runaway.

a)

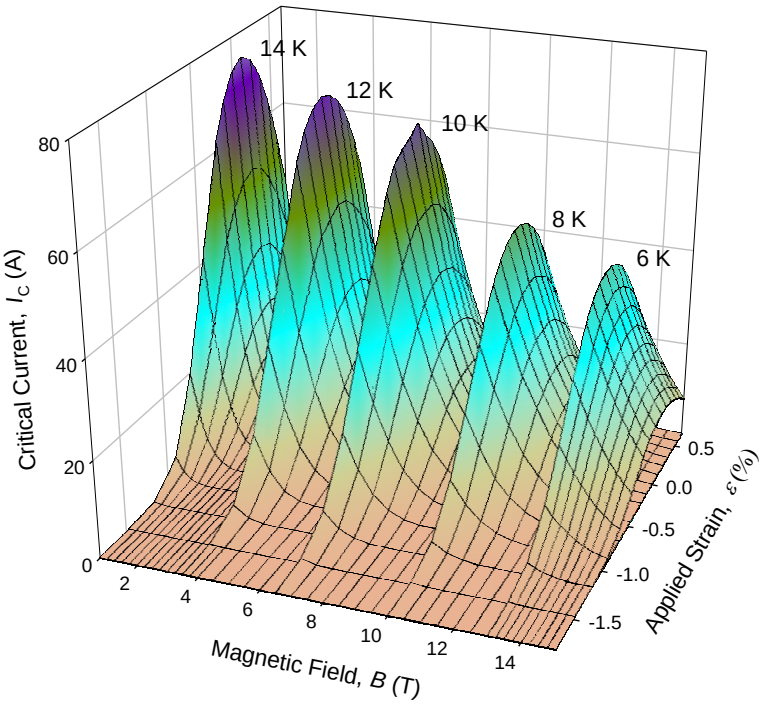
14 K
12 K
10 K
8 K
6 K
Critical Current, I_C (A)
80
60
40
20
0
2
4
6
8
10
12
14
Magnetic Field, B (T)
0.5
0.0
-0.5
-1.0
-1.5
Applied Strain, ε (%)

b)

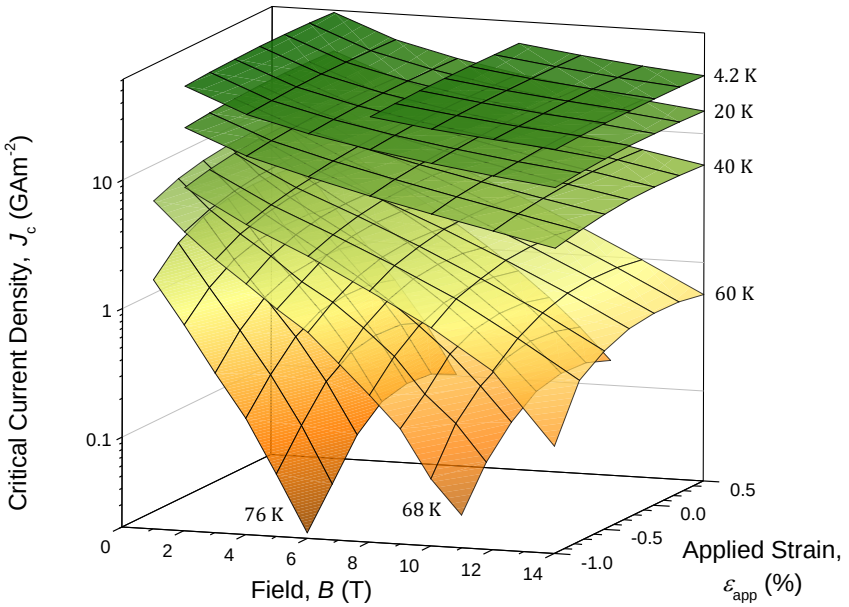
4.2 K
20 K
40 K
60 K
76 K
68 K
Critical Current Density, J_c (GAm^{-2})
10
1
0.1
0
2
4
6
8
10
12
14
Field, B (T)
0.5
0.0
-0.5
-1.0
Applied Strain, ε_{app} (%)

Figure 11: The three-dimensional critical current surface as a function of magnetic field, temperature and strain: a) Nb_3Al strand (Keys, Koizumi et al., 2002) b) Rare earth-123 Courtesy of P. Branch *et. al*. (Branch, Osamura et al., 2017).

Tables

Specification parameter	Nb_3Sn parameter value	NbTi parameter value
Cryogenic measurements		
Critical current at 12 T (6.4 T for NbTi) and 4.22 K (10 μVm^{-1})	> 190 A	> 306 A
n-value at 12 T and 4.22 K (between 10 and 100 μVm^{-1})	> 20	> 20
Hysteresis losses ±3 T (±1.5 T for NbTi) at 4.22 K	< 500 mJ/cm^3	< 55 mJ/cm^3
Residual resistivity ratio at 273 K and 20 K	> 100	> 100
Room temperature measurements		
Strand diameter	0.820 ± 0.005 mm	0.730 ± 0.005 mm
Strand twist pitch	15 ± 2 mm	15 ± 2 mm
Chromium (Nb3Sn), Nickel (NbTi) plating thickness	2 (+0 or – 1) μm	2 (+0 or – 1) μm
Cu to non-Cu ratio	1 ± 0.1	1.55 – 1.75

Table 1: Typical specification parameters and their values for the Nb_3Sn and NbTi strands being used in the ITER toroidal and poloidal magnet systems (Sborchia, Barbero Soto et al., 2011).

References

(1995) VAMAS Technical Working Party for Superconducting Materials - Recommended standard method for determination of d.c. critical current of Nb_3Sn multifilamentary composite superconductor. Cryogenics 35 S105.

(2012) CRC Handbook of Chemistry and Physics, 93 Edition: CRC Press.

(accessed 2016) ITER, the way to new energy. www.iter.org. In.

Allen PB, Dynes RC (1975) Transition temperature of strong-coupled superconductors reanalyzed. Physical Review B 12:905-922.

Antesberger G, Ullmaier H (1975) Experimental Contribution to the Summation Problem of Pinning Forces in Type-II Superconductors. Physical Review Letters 35:59-62.

Awaji S et al. (2017) First performance test of a 25 T cryogen-free superconducting magnet. Supercond Sci Technol 30:065001.

Aymar R, Barabaschi P, Shimomura Y, ITER design team (2002) The ITER design. Plasma Physics and Controlled Fusion 44:519-565.

Baixeras J, Fournet G (1967) Pertes par deplacement de vortex dans un supraconducteur de type II non ideal. J Phys Chem Solids 28:1541-1547.

Bardeen J, Stephen MJ (1965) Theory of the Motion of Vortices in Superconductors. Physical Review 140:A1197-A1207.

Bardeen J, Cooper LN, Schrieffer JR (1957) Theory of Superconductivity. Physical Review 108:1175-1204.

Branch P, Osamura K, Hampshire DP (2017) Multimodal strain dependence of the critical parameters in high-field technological superconductors Submitted to Journal.

Branch PJ, Tsui Y, Osamura K, Hampshire DP (2019) Weakly-Emergent Strain-Dependent Properties of High Field Superconductors. Accepted by Nature Scientific Reports.

Bruzzone P (2004) The index *n* of the voltage–current curve, in the characterization and specification of technical superconductors. Physica C 401:7-14.

Byrne PJP (2017) An ab-initio study of superconductors using perturbations. Thesis: Durham University.

Cai XY, Polyanskii A, Li Q, Riley GN, Larbalestier DC (1998) Current-limiting mechanisms in individual filaments extracted from superconducting tapes. Nature 392:906-909.

Campbell AM, Evetts JE, Dew-Hughes D (1968) Pinning of flux vortices in Type II superconductors. Philosophical Magazine 18:313-343.

Carbotte JP (1990) Properties of Boson-Exchange Superconductors. Reviews of Modern Physics 62:1027-1157.

Carty GJ, Hampshire DP (2008) Visualising the mechanism that determines the critical current density in polycrystalline superconductors using time-dependent Ginzburg-Landau theory. Physical Review B 77:172501.

Carty GJ, Hampshire DP (2013) The critical current density of an SNS junction in high magnetic fields. Superconductor Science and Technology 26:065007.

CERN (2013) The superconducting magnet of the big european bubble chamber (BEBC) http://cds.cern.ch/record/850617/files/. In.

Cheggour N, Hampshire DP (1997) The role of vortex melting and inhomogeneities in the transport properties of Nb3Sn superconducting wires. Inst Phys Conf Ser No 158:1275-1278.

Cheggour N, Hampshire DP (1999) Unifying the strain and temperature scaling laws for the pinning force density in superconducting niobium-tin multifilamentary wires. Journal of Applied Physics 86:552-555.
Cheggour N, Hampshire DP (2000) A probe for investigating the effect of magnetic field, temperature and strain on transport critical currents in superconducting tapes and wires. Review of Scientific Instruments 71:4521.
Clark AF (1983) Thermal expansion. In: Materials at Low Temperatures (Reed RP, Clark AF, eds), pp 75-132. Metals Park, OH: American Society for Metals.
Clark AF, Fujii G, Ranney MA (1981) The thermal expansion of several materials for superconducting magnets. IEEE Transactions on Magnetics 17:2316-2319.
Clark RG, Jones H (1986) The combination of dilution refrigerators and superconducting/hybrid magnets in physics research. ICEC 11:414-418.
Conectus (2001) Worldwide Markets for Superconductivity & Market Shares for Low-Tc / High-Tc Superconductors. In: http://conectus.org/market/.
Dew-Hughes D (1974) Flux pinning mechanisms in type II superconductors. Philosophical Magazine 30:293-305.
Dew-Hughes D (2001) The critical current of superconductors: an historical review. Low Temp Phys 27:713-722.
Dimos D, Chaudhari P, Mannhart J, LeGoues FK (1988) Orientation Dependence of Grain-Boundary Critical Currents in $YBa_2Cu_3O_{7-d}$ Bicrystals. Physical Review Letters 61:219-222.
Durham-Superconductivity-Group http://wwwduracuk/superconductivitydurham/.
Durrell JH (2009) Importance of low-angle grain boundaries in YBCO coated conductors. Supercond Sci Technol 22:013001.
Duyn JH (2012) The future of ultra-high field MRI and fMRI for study of the human brain. Neuroimage 62:1241.
Edelman HS, Larbalestier DC (1993) Resistive transitions and the origin of the n value in superconductors with a gaussian critical-current distribution. Journal of Applied Physics 74:3312-3315.
Ekin JW (1978) Current transfer in multifilamentary superconductors. I Theory. Journal of Applied Physics 49:3406-3409.
Ekin JW (1980) Strain scaling law for flux pinning in practical superconductors. Part I: Basic relationship and application to Nb_3Sn conductors. Cryogenics 20:611-624.
Ekin JW (1987) Effect of transverse compressive stress on the critical cuurent and upper critical field of Nb_3Sn. Journal of Applied Physics 62:4829-4834.
Ekin JW (1989) Offset criterion for determining superconductor critical current. Applied Physics Letters 55:905-907.
Ekin JW, Finnemore DK, Li Q, Tenbrink J, Carter W (1992) Effect of axial strain on the critical current of Ag-sheathed Bi-based superconductors in magnetic fields up to 25 T. Applied Physics Letters 61:858-860.
Ekin JW, Cheggour N, Goodrich LF, Splett J, Bordini B, Richter D (2016) Unified Scaling Law for flux pinning in practical superconductors: II. Parameter testing, scaling constants, and the Extrapolative Scaling Expression Supercond Sci and Technol 29:1-38.
Feigel'man MV, Geshkenbein VB, Larkin AI, Vinokur VM (1989) Theory of collective flux creep. Physical Review Letters 63:2303-2306.

Friend CM, Hampshire DP (1993) Transverse and longitudinal critical current densities in Nb46wt%Ti multifilamentary wire from 2 K up to T_c in magnetic fields up to 15 Tesla. In: Applied Superconductivity (Freyhardt HC, ed), pp 23 -26: DGM Informationsgesellschaft mbH.

Friend CM, Hampshire DP (1995) A probe for the measurement of the transport critical current density of superconductors in high magnetic fields and at temperatures between 2 and 150 K. Measurement Science and Technology 6:98-106.

Frost AJ, Jones H, Belenli I (1992) Design, construction and development of an apparatus for the transport-current characterization of high-temperature superconductors at a range of temperatures and magnetic fields. Cryogenics 32:1014.

Fukutsuka T, Horiuchi T, Monju Y, Tatara I, Maeda Y, Moritoki M (1984) Effects of hot isostatic pressing on the superconducting properties of Nb_3Sn multifilamentary wires. Adv Cryo Eng 30:891- 898.

G. Grasso RF (1997) Development of rectangular Bi(2223) wires with reduced anisotropy. Supercond Sci Technology 10:223.

Goldacker W, Specking W, Weiss F, Rimikis G, Flukiger R (1989) Influence of transverse, compressive and axial tensile stress on the superconductivity of $PbMo_6S_8$ and $SnMo_6S_8$ wires. Cryogenics 29:955-960.

Goldacker W, Keßler J, Ullmann B, Mossang E, Rikel M (1995) Axial tensile, transverse compressive and bending strain experiments in Bi(2223)/AgMg single core tapes. IEEE Transaction on applied superconductivity 5:1834.

Goodrich LF (1991) High Tc superconductor voltage-current simulator and the pulse method of measuring critical current. Cryogenics 31:720.

Goodrich LF (1999/2000) Critical-current measurements methods for oxide superconductor tapes and wires.

Goodrich LF, Fickett FR (1982) Critical current measurements: a compendium of experimental results. Cryogenics 22:225-241.

Goodrich LF, Bray SL (1989) Integrity tests for high-Tc and conventional critical-current measurement systems. Adv Cryo Eng (Mater) 36A:43.

Goodrich LF, Srivastava AN (1990) Software techniques to improve data reliability in superconductor and low-resistance measurements. Journal Res Natl Inst Stand Technol 95:575-589.

Goodrich LF, Srivastava AN (1992) Comparison of transport critical current measurements methods. Adv Cryo Eng (Mater) 38:559-565.

Goodrich LF, Srivastava AN (1995a) Critical current measurement methods : quantitative evaluation. Cryogenics 35 S19.

Goodrich LF, Srivastava AN (1995b) Thermal contraction of materials used in Nb3Sn critical current measurements. In: Cryogenics.

Goodrich LF, Ekin JW, Fickett FR (1982) Effect of twist pitch on short-sample V-I charactersitics of multifilamentary superconductors. Advances in Cryogenic Engineering 28:571-580.

Goodrich LF, Bray SL, Stauffer TC (1990) Thermal contraction of fibreglass-epoxy sample holders used for Nb_3Sn critical-current measurements. Adv Cryo Eng (Mater) 36:117.

Goodrich LF, Medina LT, Stauffer TC (1998) High critical-current measurements in liquid and gaseous helium. Adv Cryo Eng 44:873-880.

Goodrich LF, Srivastava AN, Yuyami M, Wada H (1992) n-value and second derivative of the superconductor voltage-current characteristic. IEEE Transactions on Applied Superconductivity 3:1265-1268.
Goodrich LF, Vecchia DF, Pittman ES, Ekin JW, Clark AF (1984) Critical current measurements on a NbTi superconducting wire standard reference material. In, pp 1-54. Boulder: N.B.S. special publication.
Goodrich LF, Wiejaczka JA, Srivastava AN, Stauffer TC, Medina LT (1995) USA interlaboratory comparison of superconductor simulator critical current measurements. IEEE Transaction on applied superconductivity 5:548.
Gould D, Wada H (1995) Introduction. Cryogenics 35:S7.
Goyal A, Paranthaman MP, Schoop U (2004) The RABiTS Approach: Using Rolling-Assisted Biaxially Textured Substrates for High-Performance YBCO Superconductors. MRS Bulletin 29:552-561.
Hampshire DP (2017) A crossboard for making two-dimensional strain measurements on high field superconductors. Private communication.
Hampshire DP, Jones H (1985) Critical current of a NbTi reference material as a function of field and temperature. Magnet Technology 9:531-535.
Hampshire DP, Jones H (1987a) Analysis of the general structure of the *E-I* characteristic of high current superconductors with particular reference to a NbTi SRM wire. Cryogenics 27:608-616.
Hampshire DP, Jones H (1987b) A detailed investigation of the E-J characteristic and the role of defect motion within the flux-line lattice for high-current-density, high field superconducting compounds with particular reference to data on Nb_3Sn throughout its entire field-temperature phase space. J Phys C - Solid State 20:3533-3552.
Hampshire DP, Jones H (1987c) Flux flow in high-temperature type II superconductors governed by the activation of Frank-Read sources and the resultant motion of core dislocations. J Phys C - Solid State 21:419-427.
Hampshire DP, Jones H, Mitchell EWJ (1985) An in-depth characterisation of $(NbTa)_3Sn$ filamentary superconductor. IEEE Transactions on Magnetics 21:289-292.
Hampshire DP, Clark AF, Jones H (1989) Flux pinning and scaling laws for superconducting V_3Ga. Journal of Applied Physics 66:3160-3167.
Hampshire RG (1974) The critical current density of Nb-60 at% Ti and Nb-25 at% Zr superconductors in small magnetic fields. Journal of Physics D - Applied Physics 7:1847-1863.
Hazelton D (2013) Presentation Spring MRS 2013: 2G HTS Conductor Development at SuperPower for Magnet Applications. http://wwwsuperpower-inccom/system/files/2013_0402+Spring+MRS+Meeting_Hazeltonpdf.
Helfand E, Werthamer NR (1966) Temperature and purity dependence of the superconducting criticial field, H_{C2}. II. Physical Review 147:288-294.
Herrmann PF (1998) Current leads. In: Handbook of Applied Superconductivity (Seeber EB, ed), p 801. Bristol: Institute of Physics.
Hole C (1995) Pulsed magnetic field characterisation of technological high temperature superconductors. Oxford University Thesis.
IEC (2006a) Superconductivity - Part 2: Critical current measurement - DC critical current of Nb_3Sn composite superconductors. In: International Standard, 1 Edition, pp IEC 61788-61782:62006: International Electrotechnical Commission.

IEC (2006b) Superconductivity - Part 3: Critical current measurement - DC critical current of Ag-sheathed Bi2212 and Bi2223 oxide superconductors. In: International Standard, pp IEC 61788-61783:62006: International Electrotechnical Commission.
IEC (2006c) Superconductivity - Part 1: Critical current measurement - DC critical current of Nb-Ti composite superconductors. In: International Standard, pp IEC 61788-61781:62006: International Electrotechnical Commission.
IEC (2015) Superconductivity - Part 21: Superconducting wires - Test methods for practical superconducting wires - General characteristics and guidance. In: International Standard, pp IEC 61788-61721:62015.
Iijima Y, Tanabe N, Kohno O, Ikeno Y (1992) Inplane aligned YBaCuO thin-films deposited on polycrystalline metallic substrates. Applied Physics Letters 60:769-771.
Itoh K, Tanaka Y, Osamura K (1996) Round robin test for the method of critical current measurement of Nb_3Sn composite superconductor. ICMC:1787-1790.
Jakob B, Pasztor G, Bona M, Asner A (1991) Reduced sensitivity of Nb_3Sn epoxy-impregnated cable to transverse stress. Cryogenics 31:390-391.
Kamata K et al. (1992) Superconducting properties and strain effects in high fields for bronze processed multifilamentary $(Nb,Ti)_3Sn$ wires and composite processed ultrafine Nb_3Al wires. Series A - Physics, Chemistry and Metallurgy A 37:99.
Keys SA, Hampshire DP (2003) A scaling law for the critical current density of weakly and strongly-coupled superconductors, used to parameterise data from a technological Nb_3Sn strand. Superconductor Science and Technology 16:1097-1108.
Keys SA, Koizumi N, Hampshire DP (2002) The strain and temperature scaling law for the critical current density of a jelly-roll Nb_3Al strand in high magnetic fields. Superconductor Science and Technology 15:991-1010.
Kirchmayr H (1995) Effects of specimen bonding materials Cryogenics. Cryogenics 35 S95.
Kirchmayr H, Siddall MB, Smathers DB (1995) Effects of mandrel materials. Cryogenics 35:S93-S94.
Kleiner WH, Roth LM, Autler SH (1964) Bulk Solution of Ginzburg-Landau Equations for Type II Superconductors: Upper critical field region. Physical Review 133:A1226-A1227.
Kramer EJ (1973) Scaling Laws for Flux Pinning in Hard Superconductors. Journal of Applied Physics 44:1360-1370.
Kramer EJ (1975) Microstructure - Critical Current Relationships in Hard Superconductors. Journal of Electronic Materials 4:839-879.
Kresin VZ (1987) On the critical-temperature for any strength of the electron phonon coupling. Physics Letters A 122:434-438.
Kresin VZ, Gutfreund H, Little WA (1984) Superconducting state in strong coupling. Solid State Commun 51:339-342.
Küpfer H, Gey W (1977) Dependence of the critical current density of superconductors on the past history of the magnetic field and temperature. Philosophical Magazine 36:859-884.
Kuroda T, Murakami Y, Itoh K, Yuyama M, Wada H, Mao D (1998) Temperature dependence of critical current density of Nb_3Al multifilamentary wires fabricated by Nb-tube and its improved processes. Cryogenics 38:785.
Larbalestier DC et al. (2014) Isotropic round-wire multifilament cuprate superconductor for generation of magnetic fields above 30 T. Nat Mater 13:375-381.
Larkin AI, Ovchinnikov YN (1984) Collective Pinning. Physica B+C 126:187-192.

Lee PJ, Larbalestier DC (1987) Development of nanometre scale structures in composites of Nb-Ti and their effect on the superconducting critical current-density. Acta Metall 35:2523-2536.

Lee TS, Jenkins I, Surrey E, Hampshire DP (2015) Optimal design of a toroidal field magnet system and cost of electricity implications for a tokamak using high temperature superconductors. Fusion Eng Des 98-99:1072–1075.

Lu XF, Hampshire DP (2009) The Magnetic Field, Temperature and Strain Dependence of the Critical Current of a Nb_3Sn Strand Using a Six Free-Parameter Scaling Law. IEEE Trans Appl Supercond 19:2619-2623.

Lu XF, Hampshire DP (2010) The field, temperature and strain dependence of the critical current density of a powder-in-tube (PIT) Nb_3Sn superconducting strand. Supercond Sci Technol 23:025002.

Lu XF, Taylor DMJ, Hampshire DP (2008) Critical current scaling laws for advanced Nb_3Sn superconducting strands for fusion applications with six free parameters. Supercond Sci Technol 21:105016.

Luhman T, Suenaga M, Klamut CJ (1978) Influence of tensile stresses on the superconducting temperature of multifilamentary Nb_3Sn composite conductors. Adv Cryo Eng 24:325-330.

Lvovsky Y, Stautner EW, Zhang T (2013) Novel technologies and configurations of superconducting magnets for MRI. Supercond Sci Technol 26:093001.

Markiewicz WD (2004a) Invariant formulation of the strain dependence of the critical temperature T_C of Nb_3Sn in a three term approximation. Cryogenics 44:895-908.

Markiewicz WD (2004b) Elastic stiffness model for the critical temperature T_C of Nb_3Sn including strain dependence. Cryogenics 44:767-782.

Markiewicz WD (2008) Comparison of strain scaling functions for the strain dependence of composite Nb_3Sn superconductors. Supercond Sci Technol 21:054004.

Marti F, Grasso G, Huang Y, Flükiger R (1997) High critical current densities in long lengths of mono- and multifilamentary Ag-sheathed Bi(2223) tapes. IEEE Transaction on applied superconductivity 7:2215.

McMillan WL (1968) Transition Temperature of Strong Coupled Superconductors. Physical Review 167:331-344.

Meingast C, Kraut O, Wolf T, Wuhl H, Erb A, Muller-Vogt G (1991) Large a-b anisotropy of the expansivity anomaly at T_C in untwinned $YBa_2Cu_3O_7$. Physical Review Letters 67:1634-1637.

Miller JR (2003) The NHMFL 45-T Hybrid Magnet System: Past, Present, and Future. IEEE Transaction on applied superconductivity 13:1385-1390.

Mitchell N et al. (2008) The ITER magnet system. IEEE Transactions on Applied Superconductivity 18:435-440.

Muriale L, Lee E, Genovese J, Trend S, (1996) Fatality due to acute fluoride poisoning following dermal contact with hydrofluyoric acid in a Palynology laboratory. Ann Occup Hygiene 40:705-710.

Muzzi L et al. (2011) Test Results of a NbTi Wire for the ITER Poloidal Field Magnets: A Validation of the 2-Pinning Components Model. IEEE Transactions on Applied Superconductivity 21:3132-3137.

Nijhuis A, Wessel WAJ, Ilyin Y, Den Ouden A, Ten Kate HHJ (2006) Critical current measurement with spatial; periodic bwending imposed by electromagnetic force on a standard test barrel with slots. Rev Sci Instrum 77:054701.

Ochiai S, Osamura K, Watanabe K (1993) Estimation of the strength distribution of Nb_3Sn in multifilamentary composite wire from change in superconducting current due to preloading. Journal of Applied Physics 74:440-445.
Ogawa R et al. (1996) Standardisation of the test method for critical current measurement of Cu/Cu-Ni/Nb-Ti composite superconductors. ICMC:1799-1802.
Okaji M, Nara K, Kato H, Michishita K, Kubo Y (1994) Thermal expansion of some advanced ceramics applicable as specimen holders of high Tc superconductors. Cryogenics 34:163.
Orlando TP, McNiff EJ, Foner S, Beasley MR (1979) Critical fields, Pauli paramagnetic limiting, and material parameters of Nb_3Sn and V_3Si. Physical Review B 19:4545-4561.
Osamura K (1998) Present status of international standardization. ISTEC Journal 11:26.
Osamura K (2015) Standardization of Test Methods for Practical Superconducting Wires. IEEE/CSC and ESAS European Superconductivity News Forum 33:1-11.
Osamura K, Sato K, Furuto Y (1997) Standardisation of the test methods for industrial superconductors by IEC/TC90. Cryogenic Engineering 32:663.
Osamura K, Machiya S, Hampshire DP (2016) Mechanism for the uniaxial strain dependence of the critical current in practical REBCO tapes. Supercond Sci Tech 29.
Osamura K et al. (2014) Uniaxial strain dependence of the critical current of DI-BSCCO tapes. Superconductor Science and Technology 27:085005.
Pobell F (1996) Matter and Methods at Low Temperatures: Springer.
Polak M et al. (1997) Current transfer lengths and the origin of linear components in the voltage-current curves of Ag-sheathed BSCCO components. Superconductor Science and Technology 10:769-777.
Pugnat P et al. (2014) Progress Report on the 43 T Hybrid Magnet of the LNCMI-Grenoble. IEEE Transaction on applied superconductivity 24.
Raine MJ, T B, Hampshire DP (2017) Measurements on large quantities of NbTi and Nb_3Sn wire for the ITER programme. In progress.
Richens PE, Jones H, van Cleemput M, Hampshire DP (1997) Strain dependence of critical currents in commercial high temperature superconductors. IEEE Transactions on Applied Superconductivity 7:1315-1318.
Ridgeon FJ, Raine MJ, Halliday DP, Lakrimi M, Thomas A, Hampshire DP (2017) Superconducting Properties of Titanium Alloys (Ti-64 and Ti-6242) for Critical Current Barrels. IEEE Transactions on Applied Superconductivity 27:1-5.
Rupp G (1977) Improvement of critical current of multifilamentary Nb_3Sn conductors under tensile-stress. IEEE Transactions on Applied Superconductivity 13:1565-1567.
Ryan DT (1997) Critical currents of commercial superconductors in the picovolt per metre electric field regime. Thesis: Oxford University.
Ryan DT, Jones H, Timms W, Kiloran N (1997) Critical current measurements at electric fields in the $pV.m^{-1}$ regime. IEEE Transactions on Applied Superconductivity 7:1455-1458.
Sakurai A, Shiotsu M, Hata K (1996) Boiling Phenomenon due to quasi-steadily and rapidly increasing heat inputs in LN_2 and LHe I. Cryogenics 36:189-196.
Sato K (2017) BSCCO wire. http://global-seicom/super/hts_e/indexhtml.
Sborchia C, Fu Y, Gallix R, Jong C, Knaster J, Mitchell N (2008) Design and specifications of the ITER TF coils. IEEE Transactions on Applied Superconductivity 18:463-466.
Sborchia M et al. (2011) Overview of ITER Magnet System and European Contribution. IEEE/NPSS 24th Symposium on Fusion Engineering:1-8.

Schlachter SI, Goldacker W, Frank A, Ringsdorf B, Orschulko H (2006) Properties of MgB_2 superconductors with regard to space applications. Cryogenics - 2005 Space Cryogenics Workshop 46:201-207.

Sneary AB, Friend CM, Vallier JC, Hampshire DP (1999) Critical current density of Bi-2223/Ag multifilamentary tapes from 4.2K up to 90K in magnetic fields up to 23T. IEEE Transactions on Applied Superconductivity 9:2585-2588.

Sugano M, Shikimachi K, Hirano N, Nagaya S (2010) The reversible strain effect on critical current over a wide range of temperatures and magnetic fields for YBCO coated conductors. Superconductor Science and Technology 23:085013.

Sunwong P, Higgins JS, Hampshire DP (2014) Probes for investigating the effect of magnetic field, field orientation, temperature and strain on the critical current density of anisotropic high-temperature superconducting tapes in a split-pair 15 T horizontal magnet. The Review of scientific instruments 85:065111.

Sunwong P, Higgins JS, Tsui Y, Raine MJ, Hampshire DP (2013) The critical current density of grain boundary channels in polycrystalline HTS and LTS superconductors in magnetic fields. Superconductivity Science and Technology 26:095006.

SuperPower-Furukawa (2013) SuperPower 2G HTS Coated Conductors. wwwsuperpower-inccom/content/2g-hts-wire.

Tachikawa K (1995) Critical current measurement method for Nb3Sn multifilamentary composite conductors. Foreward Cryogenics 35 S5.

Takeuchi T et al. (1997) Strain effects in Nb3Al multifilamentary conductors prepared by phase transformation from bcc supersaturated solid solution. Applied Physics Letters 71:122-124.

Taylor DMJ, Hampshire DP (2005a) Relationship between the *n*-value and critical current in Nb_3Sn superconducting wires exhibiting intrinsic and extrinsic behaviour. Superconductor Science and Technology 18:S297-S302.

Taylor DMJ, Hampshire DP (2005b) The scaling law for the strain dependence of the critical current density in Nb_3Sn superconducting wires. Superconductor Science and Technology 18:S241-S252.

Taylor DMJ, Hampshire DP (2005c) Properties of helical springs used to measure the axial strain dependence of the critical current density in superconducting wires. Superconductor Science and Technology 18:356-368.

Taylor DMJ, Keys SA, Hampshire DP (2002) *E-J* characteristics and *n*-values of a niobium-tin superconducting wire as a function of magnetic field, temperature and strain. Physica C 372:1291-1294.

ten Haken B (1994) Strain effects on the critical properties of high-field superconductors. In: Physics Department: University of Twente.

ten Haken B, Godeke A, ten Kate HHJ (1995) The influence of compressive and tensile axial strain on the critical properties of Nb_3Sn conductors. IEEE Transactions on Applied Superconductivity 5:1909-1912.

ten Haken B, Godeke A, ten Kate HHJ (1999) The strain dependence of the critical properties of Nb_3Sn conductors. Journal of Applied Physics 85:3247-3253.

ten Kate HHJ, Weijers HW, van Oort JM (1992) Critical current degradation in Nb_3Sn cables under transverse pressure. IEEE Transactions on Applied Superconductivity 3:1334-1337.

Trociewitz UP et al. (2011) 35.4 T field generated using a layer-wound superconducting coil made of (RE)$Ba_2Cu_3O_{7-x}$ (RE = rare earth) coated conductor. Applied Physics Letters 99:202506.

Tsui Y, Hampshire DP (2012) Critical current scaling and the pivot-point in Nb 3 Sn strands. Superconductor Science and Technology 25:054008.

Tsui Y, Surrey E, Hampshire DP (2016) Soldered Joints - an essential component of demountable high temperature superconducting fusion magnets. Supercond Sci and Technology 290:075005.

Uemura et al YJ (1989) Universal Correlations between T_C and n_s/m (Carrier Density over Effective Mass) in High-T_C Cuprate Superconductors. Physical Review Letters 62:2317-2320.

Uemura YJ et al. (1991) Basic Similarities among Cuprate, Bismuthate, Organic, Chevrel-Phase, and Heavy-Fermion Superconductors shown by Penetration-Depth Measurements. Physical Review Letters 66:2665-2668.

Varley C-R (2016) The UK Met Office. http://wwwmetofficegovuk/public/weather.

Wada H, Goodrich LF, Walters C, Tachikawa K (1995) Second intercomparison of critical current measurements. Cryogenics 35:S65-S80.

Walters CR, Davidson IM, Tuck GE (1986) Long sample high sensitivity critical current measurements under strain. Cryogenics 26:406-412.

Wang G, Raine MJ, Hampshire DP How Resistive Must Grain-Boundaries be to Limit J_C in Polycrystalline Superconductors? Submitted to Super Sci and Tech.

Wang G, Raine MJ, Hampshire DP (2017) How Resistive Must Grain-Boundaries be to Limit J_C in Polycrystalline Superconductors? Superconductor Science and Technology 30:104001.

Warnes WH (1988) A model for the resistive critical current transition in composite superconductors. Journal of Applied Physics 63:1651-1662.

Warnes WH, Larbalestier DC (1986a) Critical current distributions in superconducting composites. Cryogenics 26:643-653.

Warnes WH, Larbalestier DC (1986b) Analytical technique for deriving the distribution of critical currents in a superconducting wire. Applied Physics Letters 48:1403-1405.

White GH (1987) Experimental techniques in low-temperature physics, 3 Edition. Oxford: Oxford University Press.

White GK (1998) Thermal Expansion. In: Handbook of Applied Superconductivity (Seeber EB, ed), p 1107. Bristol: Institute of Physics Publishing.

Wiejaczka JA, Goodrich LF (1997) Interlaboratory comparison on high temperature superconductor critical-current measurements. Journal Res Natl inst Stand technol 102:29-52.

Willen DWA, Zhu W, R CJ (1997) Selection of the offset-criterion voltage parameter and its relation to the second differential of a superconductor's voltage-current curve. Inst Phys Conf Ser No 158:1013-1016.

Wilson MN (1986) Superconducting Magnets. Oxford, UK: Oxford University Press.

Wimbush SC, Strickland NM (2017) A public database of high-temperature superconductor critical current data. IEEE Transaction on Applied Superconductivity 27:8000105.

Wördenweber R (1998) Mechanism of vortex motion in high-temperature superconductors. Rep Prog Phys 62:187 -236.

Yamada N, Nara K, Okaji M, Hokata T, Kaneko T, Sadakata N (1998) Effect of thermal cycles on thermal expansion of silver-sheathed Bi2223 tape at 10-310 K. Cryogenics 38:397.

Yamafuji K, Kiss T (1997) Current-voltage characteristics near the glass-liquid transition in high-T_C superconductors. Physica C 290:9-22.
Yoon S, Kim J, Cheon K, Lee H, Hahn S, Moon S-H 26 T 35 mm all-$GdBa_2Cu_3O_{7-x}$ multi-width no-insulation superconducting magnet. Superconductor Science and Technology 29:1-6.